ESTIMATING COVID-19 VACCINE EFFICACY VIA DYNAMIC EPIDEMIOLOGICAL MODELS–A STUDY OF TEN COUNTRIES

BY YURU ZHU[1,a], JIA GU[1,b], YUMOU QIU[2,c] AND SONG XI CHEN[3,d]

[1]*Center for Statistical Science, Peking University,* [a]*yuruzhu@pku.edu.cn;* [b]*gujia@pku.edu.cn*

[2]*Department of Statistics, Iowa State University,* [c]*yumouqiu@iastate.edu*

[3]*School of Mathematical Science and Guanghua School of Management, Peking University,* [d]*songxichen@pku.edu.cn*

The real-world performance of vaccines against COVID-19 infections is critically important to counter the pandemics. We propose a varying coefficient stochastic epidemic model to estimate the vaccine efficacy based on the publicly available epidemiological and vaccination data. To tackle the challenges posed by the unobserved state variables, we develop a multi-step decentralized estimation procedure that uses different data segments to estimate different parameters. A B-spline structure is used to approximate the underlying infection rates and to facilitate model simulation in obtaining an objective function between the imputed and the simulation-based estimates of the latent state variables, leading to simulation-based estimation of the diagnosis rate using data in the pre-vaccine period and the vaccine effect parameters using data in the post-vaccine periods. And the time-varying infection, recovery and death rates are estimated by kernel regressions. We apply the proposed method to analyze the data in ten countries which collectively used 8 vaccines. The analysis reveals that the average effectiveness of the full vaccination was at least 22% higher than that of the partial vaccination and was largely above the WHO recognized level of 50% before November 20, 2021, including the Delta variant dominated period.

1. Introduction. The COVID-19 pandemic has been raging around the globe for more than two years, which has caused waves of infections and deaths among countries. The pandemic has prompted the development of vaccines which have been clinically administrated in various countries since early 2021. Ten COVID-19 vaccines had been approved for public use by the World Health Organization (WHO) as of January 2022. Vaccine makers have provided clinical trial results on the effectiveness of their products. The vaccine effectiveness against the original SARS-Cov-2 strain from recent studies is reported in Table S1, which ranged from 50.7% to 95% for the two-dose vaccination. However, SARS-CoV-2 has undergone progressive changes. The Delta variant has caused global pandemics with a high transmission rate (Planas et al., 2021), resulting in considerable socioeconomic burden and pressure on hospital systems (Liu et al., 2021).

There is a great need to evaluate the vaccine efficacy (VE) in the real-world situation. Clinical trials used to evaluate the VE exclude certain part of the population and are difficult to control all confounding factors that may cause infections in the population. The retrospective studies, such as Li et al. (2021), used the proportion of the vaccine breakthrough cases in all infected cases in specific institutions, which typically had a small sample size relative to the daily infections in a country. Moreover, most countries do not collect vaccine breakthrough statistics, which brings great challenges for evaluating vaccine effects in real-world situations. In addition, many studies have only provided data on effectiveness against symptomatic cases as including asymptomatic ones is difficult. Hence, the real-world performance against any infection is an important issue.

Keywords and phrases: Reproduction number, Scenario analysis, Simulation-based estimation, Stochastic epidemic model, Varying coefficient model.

Compartmental models, like SIR (Kermack and McKendrick, 1927) and SEIR (Anderson and May, 1982) models, are widely used for modeling the transmission of infectious diseases, which divide a population into compartments and specify the transition rates among compartments by ordinary differential equations (ODEs). Stochastic epidemic models (SEMs) extended from the SEIR model had been proposed to study the spread of COVID-19 before vaccines were available (Hao et al., 2020; Tian et al., 2021; Yan et al., 2021). As asymptomatic and pre-symptomatic infections in the COVID-19 pandemic are not observable, the likelihood functions based on the observed data are rather complex due to having to integrate out unobserved state variables. Bayesian methods which target the joint posterior distribution of the unobserved data and the model parameters use the Markov chain Monte Carlo (Auranen et al., 2000) or the sequential Monte Carlo (Dukic, Lopes and Polson, 2012) for parameter estimation. Quick, Dey and Lin (2021) built a multilevel regression model on the COVID-19 daily confirmed infection counts, polymerase chain reaction testing and serological survey data, and developed an EM algorithm to estimate the model parameters.

There are recent studies (Dashtbali and Mirzaie, 2021; Giordano et al., 2021) in evaluating COVID-19 vaccination strategies using a deterministic compartment model that assumes a portion of the vaccinated can achieve permanent and full immunity, which is quite restrictive. Moreover, deterministic models are inadequate to facilitate statistical inference on the characteristics of epidemics. Incorporating stochasticity into epidemic models is needed for real-world evaluation due to the randomness of the state variables. There has been no study using the publicly available data to estimate the real-world COVID-19 VE without the restrictive permanent and full immunity assumption and incorporating the stochastic natures of the epidemics and the unobservable asymptomatic and pre-symptomatic cases.

We propose a new SEM for evaluating COVID-19 vaccine efficacy based on the publicly available epidemiological and vaccination data, which allows breakthroughs in fully and partially immunized people, and infection before clinical diagnosis and being asymptomatic. The advantages of our proposal over the traditional cohort or case-control studies are in its much-reduced data collection cost and timely assessment on the real-world performance of vaccines.

The unavailability of data on breakthrough cases and infections before clinical confirmation brings challenges to estimating real-world vaccine effects. To tackle the challenges, this study proposes a decentralized estimation approach that utilizes different periods of the data series for estimating different parameters, taking advantage of long observations of the COVID-19 epidemics. Unobservable compartments are imputed by data on observed compartments based on the proposed stochastic model. A major part of the estimation is attained by minimizing certain contrast functions between the imputed and the simulation-based estimates for the infected to estimate (i) the diagnosis rate using the pre-vaccine period data, and (ii) the vaccine effect parameters using the post-vaccine period data. The final time-varying infection rate is estimated by the kernel smoothing method based on the model-implied imputation equations.

We apply the proposed model and estimation approach to analyze the data from ten countries to estimate the real-world VEs and other key parameters. It is found that the VEs of partial (one dose) vaccination ranged from 48% to 64% and 17.5% to 48% in the pre-Delta and the Delta dominated periods, respectively. The VEs of the full (usually two-dose) vaccination ranged from 68% to 95% in the pre-Delta era, which were reduced to 45% to 74% when the Delta variant dominated. The average VEs from the full vaccination were at least 22% more than those of the partial vaccination, suggesting significant extra protection offered by the full vaccination. Furthermore, the full vaccination efficacy for the 10 countries up to November 20, 2021 (before the Omicron era) was largely above the WHO recognized 50% level with all 8 brands of the vaccines, including inactivated vaccines. Our results of the

mixed effectiveness of vaccines being administrated simultaneously in a country were consistent with those of published studies via clinical trials and the retrospective studies reviewed in the supplementary material (SM).

The organization of this paper is as follows. Section 2 introduces the data used in this study and the periods with respect to vaccination and the pandemic. Section 3 presents the proposed stochastic epidemic model with vaccination compartments. The multi-step decentralized estimation and inference procedure is given in Section 4. Section 5 reports simulation results to evaluate the proposed method. Sections 6 and 7 provide the empirical analysis on the estimated vaccine effects in three periods of the pandemic, and the scenario analysis results for the no-vaccine, partial-vaccination and first-dose-priority scenarios, respectively. Section 8 concludes the paper.

2. Data. We analysed the publicly available epidemiological data from February 23, 2020 to November 20, 2021 of 10 countries listed in Table S3 of the SM. The first date marked the start of the local transmission in these countries, while the second date represented the end of the pre-Omicron era as Omicron was first reported on November 24, 2021. The daily epidemiological statistics were obtained from "the 2019 Novel Coronavirus Visual Dashboard" at Johns Hopkins University, and the information on the vaccine types and the cumulative numbers of people receiving one or two vaccine doses was obtained from the official statistics of the countries. In this paper, the full dose means one dose in the case of Janssen and two doses for the other brands.

Some countries (Canada, Italy, Portugal, the UK, the US) under-reported their daily recovery cases almost from the beginning of the pandemics (Yan et al., 2021) as reflected in Figure S1 of the SM. Moreover, recoveries in all the 10 countries have not been reported since August, 2021. Thus, we used 14 days as the average time of recovery, as suggested by WHO and supported clinically by Guan et al. (2020), to impute the recovered cases for these countries. The daily data were smoothed to reduce potential measurement errors using the procedure outlined in the SM.

For each country, we studied four sequential and non-overlapping periods of the pandemic: the pre-vaccine period from the start of the epidemic till the start of vaccination, the pre-Delta period till the Delta variant was first detected in the country, the intervening period till the Delta variant became predominant and the Delta dominated period when the majority of the cases were caused by the Delta variant. India did not have the pre-Delta period as its first Delta case was reported before vaccination. The dates of the periods in the countries are provided in the SM.

3. Epidemiological Model. We propose a new SEM called varying coefficient susceptible-vaccinated-infected-diagnosed-removed (vSVIADR) model with ten compartments for a well-mixed population of size M. The proposed model with its compartments and key parameters is illustrated in Figure 1. It shows that in addition to the latent asymptomatic and pre-symptomatic compartments before diagnosis considered in Yan et al. (2021), we add the partially and fully vaccine immunized compartments to model the transmission after vaccination. This allows to estimate the VE in real-world situations using daily statistics of epidemics and vaccination. As the types, supplies and distribution strategies of vaccines vary from country to country, such an estimation would better reflect the actual VE in a given population than the estimates from the experimental studies using clinical trial data (Voysey et al., 2021; Polack et al., 2020) or the retrospective studies (Sheikh et al., 2021; Li et al., 2021).

Let $V_0(t)$, $V_1(t)$, $V_2(t)$, $V_e(t)$ be counts at day t of four uninfected sub-populations having received no vaccine, with partial, full and expired vaccine immunity; and $I_a(t)$ and

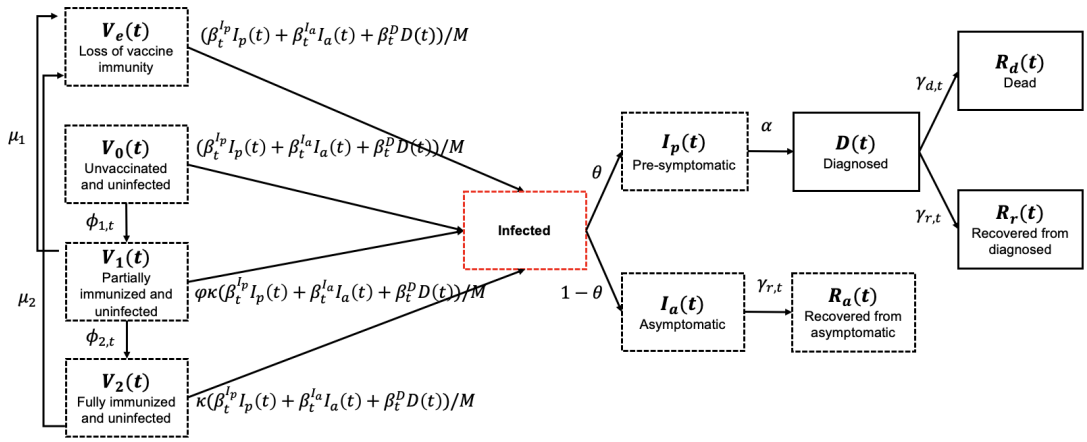

Fig 1: Compartments and state variables with a dynamic flow chart of the proposed vSVIADR model. The observable (unobservable) compartments are marked by solid (dashed) boxes. The red dashed infected box is a mix of pre-symptomatic and asymptomatic infections.

$I_p(t)$ be the counts of asymptomatic and pre-symptomatic infections, respectively, where the asymptomatic cases are never diagnosed, and the pre-symptomatic cases will be tested and confirmed in a future date, but not yet diagnosed at time t. The latter two compartments start two epidemiological pathways with that from asymptomatic $I_a(t)$ leading to the self recovered $R_a(t)$, and the symptomatic pathway from $I_p(t)$ to the diagnosed $D(t)$, then to the recovered $R_r(t)$ and the dead $R_d(t)$. We combine V_0 and V_e into one state S, and let $S(t) = V_0(t) + V_e(t)$ be the counts of uninfected people without vaccine immunity whether due to receiving no vaccine or losing vaccine immunity at day t, $\mathcal{F}_t = \sigma((S(s), V_1(s), V_2(s), I_a(s), I_p(s), D(s), R_a(s), R_r(s), R_d(s)), s \leq t)$ be the σ-algebra generated by the counts of all compartments up to time t and $\Delta A(t) = A(t+1) - A(t)$ be the daily increment operator of a state variable A on day t.

Let $H(t, \boldsymbol{\beta}_t) = \{\beta_t^{\mathrm{I}_a} I_a(t) + \beta_t^{\mathrm{I}_p} I_p(t) + \beta_t^{\mathrm{D}} D(t)\}/M$ be the total infection loading at t, where $\boldsymbol{\beta}_t = (\beta_t^{\mathrm{I}_a}, \beta_t^{\mathrm{I}_p}, \beta_t^{\mathrm{D}})$. The vSVIADR model prescribes the following conditional mean model

$$
\begin{aligned}
&\mathrm{E}\{\Delta S(t)|\mathcal{F}_t\} = -H(t, \boldsymbol{\beta}_t) S(t) - \phi_{1,t} V_0(t) + \mu_1 V_1(t) + \mu_2 V_2(t),\\
&\mathrm{E}\{\Delta V_1(t)|\mathcal{F}_t\} = \phi_{1,t} V_0(t) - \mu_1 V_1(t) - \varphi\kappa H(t, \boldsymbol{\beta}_t) V_1(t) - \phi_{2,t} V_1(t),\\
&\mathrm{E}\{\Delta V_2(t)|\mathcal{F}_t\} = \phi_{2,t} V_1(t) - \mu_2 V_2(t) - \kappa H(t, \boldsymbol{\beta}_t) V_2(t),\\
&\mathrm{E}\{\Delta I_a(t)|\mathcal{F}_t\} = (1-\theta) H(t, \boldsymbol{\beta}_t)\{S(t) + \varphi\kappa V_1(t) + \kappa V_2(t)\} - \gamma_{r,t} I_a(t),\\
&\mathrm{E}\{\Delta I_p(t)|\mathcal{F}_t\} = \theta H(t, \boldsymbol{\beta}_t)\{S(t) + \varphi\kappa V_1(t) + \kappa V_2(t)\} - \alpha I_p(t),\\
&\mathrm{E}\{\Delta D(t)|\mathcal{F}_t\} = \alpha I_p(t) - \gamma_t D(t),\ \mathrm{E}\{\Delta R_a(t)|\mathcal{F}_t\} = \gamma_{r,t} I_a(t),\\
&\mathrm{E}\{\Delta R_r(t)|\mathcal{F}_t\} = \gamma_{r,t} D(t) \text{ and } \mathrm{E}\{\Delta R_d(t)|\mathcal{F}_t\} = \gamma_{d,t} D(t).
\end{aligned} \tag{1}
$$

This form of the model connects well with the existing compartmental models defined via ODEs dating back to the SIR and SEIR models. However, as some compartments are latent, Model (1) is not enough to determine the joint distribution of the state variables. More on the in-flow and out-flow of the state variables are needed to specify the data generation.

Let $\Delta S_I^-(t)$, $\Delta V_{1,I}^-(t)$ and $\Delta V_{2,I}^-(t)$ be the numbers of daily infected people from the three compartments S, V_1 and V_2 on day t, respectively; $\Delta V_{1,L}^-(t)$ and $\Delta V_{2,L}^-(t)$ be the daily

increments of people losing immunity from $V_1(t)$ and $V_2(t)$, respectively; and $\Delta I_a^+(t)$ be the number of daily new asymptomatic cases on day t, where $+$ $(-)$ means inflow (outflow) from a compartment. Furthermore, let $N(t) = D(t) + R_d(t) + R_r(t)$ be the accumulative confirmed cases, $G_1(t)$ and $G_2(t)$ be the accumulative numbers of people who have received at least one dose of vaccine and who are fully vaccinated, respectively.

The following is the probabilistic specification of the vSVIADR model via mutually independent Poisson distributions:

$$
\begin{aligned}
&\Delta S_I^-(t)|\mathcal{F}_t \sim \text{Poi}\{H(t,\boldsymbol{\beta}_t)S(t)\},\\
&\Delta V_{1,I}^-(t)|\mathcal{F}_t \sim \text{Poi}\{\varphi\kappa H(t,\boldsymbol{\beta}_t)V_1(t)\},\ \Delta V_{2,I}^-(t)|\mathcal{F}_t \sim \text{Poi}\{\kappa H(t,\boldsymbol{\beta}_t)V_2(t)\},\\
&\Delta I_a^+(t)|\mathcal{F}_t \sim \text{Binomial}(\Delta S_I^-(t) + \Delta V_{1,I}^-(t) + \Delta V_{2,I}^-(t), 1-\theta)\\
&\Delta G_1(t)|\mathcal{F}_t \sim \text{Poi}\{\phi_{1,t}V_0(t)\},\ \Delta G_2(t)|\mathcal{F}_t \sim \text{Poi}\{\phi_{2,t}V_1(t)\},\\
&\Delta V_{1,L}^-(t)|\mathcal{F}_t \sim \text{Poi}\{\mu_1 V_1(t)\},\ \Delta V_{2,L}^-(t)|\mathcal{F}_t \sim \text{Poi}\{\mu_2 V_2(t)\},\ \Delta N(t)|\mathcal{F}_t \sim \text{Poi}\{\alpha I_p(t)\}\\
&\Delta R_a(t)|\mathcal{F}_t \sim \text{Poi}\{\gamma_{r,t} I_a(t)\},\ \Delta R_r(t)|\mathcal{F}_t \sim \text{Poi}\{\gamma_{r,t} D(t)\},\ \Delta R_d(t)|\mathcal{F}_t \sim \text{Poi}\{\gamma_{d,t} D(t)\}.
\end{aligned}
\tag{2}
$$

The Poisson assumptions can be relaxed into other distributions to accommodate potential overdispersion as discussed in the conclusion section. Given the initial $\{S(1), V_1(1), V_2(1), I_a(1), I_p(1), D(1), R_a(1), R_r(1), R_d(1)\}$ and based on the transitional specification (2), the state variables progress according to Equation (A.3) in the SM which will be used to generate trajectories of the state variables for parameter estimation.

The infectious states in the vSVIADR model are the asymptomatic, pre-symptomatic, and diagnosed (I_a, I_p and D) with time-varying infection rates $\beta_t^{\mathrm{I}_a}$, $\beta_t^{\mathrm{I}_p}$ and β_t^{D}, respectively. Asymptomatic and pre-symptomatic cases are not diagnosed at t, and asymptomatic cases are never confirmed through the infection. Among the three infectious states, only the diagnosed is observable. Since the asymptomatic cases develop no symptom, and the diagnosed people are advised to isolate at home or hospitalized, we design a model such that the pre-symptomatic compartment is more contagious than the other two compartments. Specifically, we assume $\beta_t^{\mathrm{I}_a} = \beta_t^{\mathrm{D}} = \beta_t^{\mathrm{I}_p}/r$ for a known constant $r > 1$, which was set as 5 following the specification in Gu et al. (2020) to avoid additional computational cost. It could be made unknown and estimated by minimizing a criterion function along with α in Section 4.2.

The full vaccination (one dose for Janssen or two does for the other brands) is assumed to reduce the infection rate by a factor $\kappa \in [0,1]$ relative to the unvaccinated, while the partial vaccination reduces the rate by $\varphi\kappa$ for a $\varphi \in [0, 1/\kappa]$. The VE is $1-\kappa$ and $1-\varphi\kappa$ for the fully and partially vaccinated under the model, respectively. If the full vaccination is fully effective, then $\kappa = 0$, while $\kappa = 1$ for complete failure.

The model assumes temporary immunity via μ_1 and μ_2 as $1/\mu_1$ and $1/\mu_2$ specify the average lengths of immunity after the partial and full vaccination, respectively. As the vaccinated people with lost or expired immunity are unobservable, μ_1 and μ_2 can not be estimated from the daily epidemiological data, and their values have to be attained from clinical studies. We set $\mu_1 = 1/60$ and $\mu_2 = 1/240$ according to Doria-Rose et al. (2021) and Johnson & Johnson (2021). It is noted that Dashtbali and Mirzaie (2021) and Giordano et al. (2021) assumed $\mu_1 = \mu_2 = 0$ (permanent immunity) and a regular flow from susceptibles with full efficacy of vaccines. The time-varying vaccination rates $\phi_{1,t}$ and $\phi_{2,t}$ of the unvaccinated and uninfected, and the partially vaccine immunized and uninfected, respectively, can be estimated by the kernel smoothing on $\Delta G_1(t)$ and $\Delta G_2(t)$.

Under the vSVIADR model, $\theta \in (0,1)$ is the daily proportion of the pre-symptomatic cases and α is the diagnostic rate from the pre-symptomatic state I_p to the diagnosed state D. Implied from (2), the number of newly asymptomatic cases $\Delta I_a^+(t)$ given the daily new

infections follows Binomial$(\Delta S_I^-(t) + \Delta V_{1,I}^-(t) + \Delta V_{2,I}^-(t), 1-\theta)$. As the asymptomatic and pre-symptomatic cases are latent, similar as μ_1 and μ_2, we determine the value of θ based on existing studies. The meta-analysis of Buitrago-Garcia et al. (2020) found 20% (CI: 17% - 25%) of COVID-19 infections remained asymptomatic in 79 published studies, which led our setting $\theta = 0.8$ in the analysis.

The effective reproduction number R_t is a key indicator and quantifies the mean number of secondary infections generated per primary infection at t. Derivation in the SM shows that

$$R_t = \left\{ (1-\theta)\frac{\beta_t^{\mathrm{I}_a}}{\gamma_{r,t}} + \theta\left(\frac{\beta_t^{\mathrm{I}_p}}{\alpha} + \frac{\beta_t^{\mathrm{D}}}{\gamma_t}\right)\right\} \frac{S(t) + \varphi\kappa V_1(t) + \kappa V_2(t)}{M} \tag{3}$$

under the vSVIADR model. When $R_t > 1 (< 1)$, the epidemic is increasing (decreasing). From (3), R_t is conventionally driven positively by the three infection rates $\{\beta_t^{\mathrm{I}_a}, \beta_t^{\mathrm{I}_p}, \beta_t^{\mathrm{D}}\}$, and negatively by the diagnosis rate α, the removal rate γ_t and the VEs represented by $1-\kappa$ and $1-\varphi\kappa$. That vaccine slowing down R_t is seen by relocating $\varphi\kappa V_1(t) + \kappa V_2(t)$ from the susceptible population, as more people move from the group $S(t)$ without vaccine immunity to the partially or fully vaccinated groups $V_1(t)$ and $V_2(t)$ with enhanced immunity.

4. Estimation and inference. We consider the estimation of the model parameters α, $\beta_t^{\mathrm{I}_p}$, $\gamma_{d,t}$, $\gamma_{r,t}$, φ and κ for a country, which leads to the estimation of the effective reproduction number R_t by (3) as well as the VEs. For each country, we denote its start date of the pandemic as $t = 1$, the start date of vaccination as T_1, and the ending date as T. The observed data are $\{D(t), R_r(t), R_d(t), G_1(t), G_2(t)\}_{t=1}^T$.

Yan et al. (2021) proposed a vary-coefficient compartment model for the pre-vaccine period, and a leave-one-out cross-validation criteria with a kernel smoothing procedure for estimating model parameters. The approach no longer works for the current situation with the vaccine compartments for two reasons. First, the proposed model in (2) is more complex with more unobservable compartments than the one in Yan et al. (2021). Second, there are more parameters to optimize in an objective function, which include the diagnosis rate α, vaccine effects φ and κ, and the infection rate $\beta_t^{\mathrm{I}_p}$. New estimation method needs to be developed.

The simulation-based estimation approach has been adopted to estimate parameters in deterministic ODEs from partially observed data or data with additive measurement errors. The single (Hicks and Ray, 1971) shooting method minimizes distance measures between the observed state variables and the simulated trajectories of the variables via the ODEs with respect to the parameter values. The multiple shooting method is similar except that it breaks the time domain into smaller intervals with extra initial conditions (Baake et al., 1992). There are non-simulation-based estimation approaches for differential-equation-based models, which involve the generalized profiling estimation via B-splines expansions or the nonparametric regression estimate of model coefficients (Ramsay et al., 2007; Liang and Wu, 2008).

Our estimation faces several challenges. First of all, although the conditional means of the vSVIADR model are specified in the forms of ODEs, the estimation approaches of the ODEs with measurement errors (Liang and Wu, 2008) are not applicable for the current stochastic model with much heterogeneity due to the conditional Poisson specification. Second, the unobservable compartments in the model and the complexity of the system exhibited by (2) and (A.3) make the maximum likelihood estimation and the EM algorithm, which involves integrating out the latent variables in the conditional distribution, difficult to be implemented, although the EM algorithm had been applied for the much simpler binomial epidemic chain model (Becker, 1997). To meet these challenges, we propose a multi-step decentralized estimation procedure, which estimates the constant parameters α, φ and κ by minimizing certain

criterion functions, and estimates the time-varying parameters by the nonparametric regression method. The decentralization implies using different periods of data to estimate different parameters as shown next.

4.1. *Estimation of removal rates $\gamma_{d,t}$ and $\gamma_{r,t}$.* The estimation of the two removal parameters is the most straightforward among all the parameters, as the three compartments $D(t)$, $R_r(t)$ and $R_d(t)$ involving the recovery process are observable largely because they are located at the end of the epidemiological process. From the Poisson increments of the daily new deaths $\Delta R_d(t)$ and daily new recoveries $\Delta R_r(t)$ specified in (2), we have $\mathrm{E}\{\Delta R_d(t)|D(t)\} = \gamma_{d,t}D(t)$ and $\mathrm{E}\{\Delta R_r(t)|D(t)\} = \gamma_{r,t}D(t)$. The time-varying nature of the parameters suggests the locally weighted kernel smoothing estimator of $\gamma_{r,t}$ and $\gamma_{d,t}$ by regressing $\Delta R_r(t)$ and $\Delta R_d(t)$ on $D(t)$ without intercept, respectively. Specifically, the estimators are in the form

$$\begin{aligned} \hat{\gamma}_{d,t} &= \frac{\sum_{i=1}^{T-1} D(i)\Delta R_d(i)B((t-i)/h_d)}{\sum_{i=1}^{T-1} D(i)^2 B((t-i)/h_d)} \quad \text{and} \\ \hat{\gamma}_{r,t} &= \frac{\sum_{i=1}^{T-1} D(i)\Delta R_r(i)B((t-i)/h_r)}{\sum_{i=1}^{T-1} D(i)^2 B((t-i)/h_r)}, \end{aligned} \tag{4}$$

where $B(\cdot)$ is a boundary kernel modified from a symmetric kernel, and h_d and h_r are the temporal smoothing bandwidths; see the SM for details.

4.2. *Estimation of diagnosis rate α.* We consider using data in the pre-vaccine stage $\mathcal{S}_1 = \{t_1, \ldots, t_2\} \in \{1, \ldots, T_1\}$ to estimate the diagnosis rate α, which avoids the interference from estimating the vaccine effect parameters φ and κ. The challenge in estimating α lies in the pre-symptomatic compartment $I_p(t)$ being latent. Our strategy is to minimize a contrast measure with respect to α and $\beta_t^{\mathrm{I}_p}$ in the form of

$$f_1(\alpha, \beta_t^{\mathrm{I}_p}) = \frac{1}{|\mathcal{S}_1|} \sum_{t \in \mathcal{S}_1} \left\{ \hat{\mathrm{E}}^{\alpha}\{I_p(t)|\mathcal{F}_{t-1}\}/\hat{I}_p^{\alpha}(t) - 1 \right\}^2 \text{ for } \hat{I}_p^{\alpha}(t) = \Delta N(t)/\alpha, \tag{5}$$

where $\hat{I}_p^{\alpha}(t)$ is an imputed value of $I_p(t)$ using the daily increment $\Delta N(t)$ of confirmed cases at a given α by noting $\mathrm{E}\{\Delta N(t)|\mathcal{F}_t\} = \alpha I_p(t)$, and $\hat{\mathrm{E}}^{\alpha}\{I_p(t)|\mathcal{F}_{t-1}\}$ is a simulation-based estimate of $\mathrm{E}\{I_p(t)|\mathcal{F}_{t-1}\}$ by averaging the simulated trajectories according to (2) and (A.3) at the given α and $\beta_t^{\mathrm{I}_p}$. The construction of $\hat{\mathrm{E}}^{\alpha}\{I_p(t)|\mathcal{F}_{t-1}\}$ requires (i) obtaining initial values of all compartments at t_1 via imputation; (ii) a preliminary estimate of the time-varying infection rate $\beta_t^{\mathrm{I}_p}$ by nonparametric regression based on the imputed variables; and (iii) a B-spline enhancement to the preliminary estimate of $\beta_t^{\mathrm{I}_p}$ for better and more stable fitting of $f_1(\alpha, \beta_t^{\mathrm{I}_p})$. Throughout this section, the superscript α indicates the computed quantities depending on α.

The observable $D(t)$, $R_r(t)$ and $R_d(t)$ can be used as the initial values. For those unobservable state variables, $\hat{I}_p^{\alpha}(t)$ can serve as a replacement for $I_p(t)$. To impute $I_a(t)$, since

$$\begin{aligned} \mathrm{E}\{\Delta I_p(t)|\mathcal{F}_t\} &= \theta H(t, \boldsymbol{\beta}_t)S(t) - \alpha I_p(t) \quad \text{and} \\ \mathrm{E}\{\Delta I_a(t)|\mathcal{F}_t\} &= (1-\theta)H(t, \boldsymbol{\beta}_t)S(t) - \gamma_{r,t} I_a(t) \end{aligned} \tag{6}$$

in the pre-vaccine period, replacing $\theta H(t, \boldsymbol{\beta}_t)S(t)$ by $\Delta I_p(t) + \alpha I_p(t)$, we have $\Delta I_a(t) \approx \{\Delta I_p(t) + \alpha I_p(t)\}(1-\theta)/\theta - \gamma_{r,t} I_a(t)$. Thus, $\{I_a(t)\}$ can be imputed sequentially by

$$\hat{I}_a^{\alpha}(t) = \{\Delta \hat{I}_p^{\alpha}(t-1) + \alpha \hat{I}_p^{\alpha}(t-1)\}(1-\theta)/\theta + (1 - \hat{\gamma}_{r,t-1})\hat{I}_a^{\alpha}(t-1) \tag{7}$$

in the pre-vaccine period, where $\hat{I}_p^\alpha(t)$ is given in (5) and $\hat{\gamma}_{r,t}$ is the estimator attained in (4). Furthermore, as $\mathrm{E}\{\Delta R_a(t)|\mathcal{F}_t\} = \gamma_{r,t} I_a(t)$, $R_a(t)$ in the pre-vaccine period can be imputed by

$$\hat{R}_a^\alpha(t) = \hat{R}_a^\alpha(t-1) + \hat{\gamma}_{r,t-1}\hat{I}_a^\alpha(t-1). \tag{8}$$

Then, $S(t)$ can be imputed by $\hat{S}^\alpha(t) = M - \hat{I}_a^\alpha(t) - \hat{I}_p^\alpha(t) - N(t) - \hat{R}_a^\alpha(t)$, leading to the initial values $\hat{\mathcal{H}}^\alpha(t_1) = \{D(t_1), R_r(t_1), R_d(t_1), \hat{I}_p^\alpha(t_1), \hat{I}_a^\alpha(t_1), \hat{R}_a^\alpha(t_1), \hat{S}^\alpha(t_1)\}$ at time t_1 for a given α.

To minimize the objective function $f_1(\alpha, \beta_t^{\mathrm{I}_p})$ with respective to α and the varying coefficient $\beta_t^{\mathrm{I}_p}$ in (5), we approximate $\beta_t^{\mathrm{I}_p}$ by the B-spline

$$\tilde{\beta}_t^{\mathrm{I}_p}(\boldsymbol{\lambda}_1) = \sum_{k=0}^{n_1+3} \lambda_{1,k}\psi_{k,4}\{(t-t_1)/(t_2-t_1)\} \tag{9}$$

for $t \in \mathcal{S}_1$, where $\{\psi_{k,4}(s)\}_{k=0}^{n_1+3}$ are the order four basis functions supported on $[0,1]$, $0 \le n_1 < t_2 - t_1 - 3$ is the number of equally spaced internal knots within $[0,1]$, and $\boldsymbol{\lambda}_1 = (\lambda_{1,0}, \ldots, \lambda_{1,n_1+3})$ is the coefficient vector of the splines. This makes the objective function (5) take the form $f_1(\alpha, \tilde{\beta}_t^{\mathrm{I}_p}(\boldsymbol{\lambda}_1))$, which makes the optimization seemingly parametric. Given $\boldsymbol{\lambda}_1$, α and the initial values $\hat{\mathcal{H}}^\alpha(t_1)$, the trajectories of $I_p(t)$ can be generated from the vSVIADR model for $t \in \mathcal{S}_1$, which leads to the estimator $\hat{\mathrm{E}}^\alpha\{I_p(t)|\mathcal{F}_{t-1}\}$ and the evaluation of $f_1(\alpha, \tilde{\beta}_t^{\mathrm{I}_p}(\boldsymbol{\lambda}_1))$ as follows.

We first determine a plausible range for the parameter $\boldsymbol{\lambda}_1$ in order to minimize $f_1(\alpha, \tilde{\beta}_t^{\mathrm{I}_p}(\boldsymbol{\lambda}_1))$. To realize this task, we first construct a kernel smoothing estimator for $\beta_t^{\mathrm{I}_p}$ in the pre-vaccine period based on the imputed values $\{\hat{I}_p^\alpha(t), \hat{I}_a^\alpha(t), \hat{S}^\alpha(t)\}$. From the first equation in (6), we have

$$\{I_p(t+1) + (\alpha-1)I_p(t)\}/\theta \approx \{\beta_t^{\mathrm{I}_a} I_a(t) + \beta_t^{\mathrm{I}_p} I_p(t) + \beta_t^{\mathrm{D}} D(t)\}S(t)/M. \tag{10}$$

Let $Y(t) = \{\hat{I}_p^\alpha(t+1) + (\alpha-1)\hat{I}_p^\alpha(t)\}/\theta$ and $X(t) = \left[\hat{I}_p^\alpha(t) + \{D(t) + \hat{I}_a^\alpha(t)\}/r\right]\hat{S}^\alpha(t)/M$. Under the setting $\beta_t^{\mathrm{I}_a} = \beta_t^{\mathrm{D}} = \beta_t^{\mathrm{I}_p}/r$, from Equation (10), $\beta_t^{\mathrm{I}_p}$ in the pre-vaccine stage can be estimate by the kernel regression of $Y(t)$ on $X(t)$ as

$$\hat{\beta}_t^{\mathrm{I}_p,\alpha} = \frac{\sum_{i=1}^{T_1} X(i)Y(i)B\{(t-i)/h\}}{\sum_{i=1}^{T_1} X(i)^2 B\{(t-i)/h\}} \tag{11}$$

for $t < T_1$, where $B(\cdot)$ is the same boundary kernel used in (4) and h is a bandwidth parameter. This regression estimate of $\beta_t^{\mathrm{I}_p}$ can be interpreted by the dynamics of $I_p(t)$ from the fifth equation in (1). Note that $\alpha\hat{I}_p^\alpha(t)$ is the estimated out-flow from $I_p(t)$ to $D(t)$. Therefore, $\hat{I}_p^\alpha(t+1) - \hat{I}_p^\alpha(t) + \alpha\hat{I}_p^\alpha(t)$ is the estimated daily new pre-symptomatic cases (the inflow to $I_p(t)$). Since θ proportion of the total new infections are pre-symptomatic in the vSVIADR model, $Y(t)$ approximates the total newly infected cases (asymptomatic and pre-symptomatic combined) at time t. Meanwhile, $\hat{I}_p^\alpha(t) + \{D(t) + \hat{I}_a^\alpha(t)\}/r$ represents the estimated size of the infection group at t, where $\{D(t) + \hat{I}_a^\alpha(t)\}/r$ is the rescaled infectious stock in the D and I_a compartments in terms of $\beta_t^{\mathrm{I}_p}$. In a well-mixed population before the vaccination, the newly infected cases were caused by the contact of the infectious and susceptible people (estimated by $\hat{S}^\alpha(t)$) with the infection rate $\beta_t^{\mathrm{I}_p}$. Therefore, $\beta_t^{\mathrm{I}_p} X(t)$ can be viewed as the expected value of the newly infected number $Y(t)$.

Regressing $\hat{\beta}_t^{\mathrm{I}_p,\alpha}$ on the B-spline basis functions, we obtain a preliminary estimate of $\boldsymbol{\lambda}_1$

$$\tilde{\boldsymbol{\lambda}}_1^{\alpha} = (\tilde{\lambda}_0^{\alpha}, \ldots, \tilde{\lambda}_{n_1+3}^{\alpha}) = \underset{\boldsymbol{\lambda}_1}{\operatorname{argmin}} \sum_{t\in\mathcal{S}_1} \left[\hat{\beta}_t^{\mathrm{I}_p,\alpha} - \sum_{k=0}^{n_1+3} \lambda_{1,k}\psi_{k,4}\{(t-t_1)/(t_2-t_1)\} \right]^2. \tag{12}$$

Let the cartesian product set $\Lambda_\alpha = [\tilde{\lambda}_0^{\alpha} - \delta_1, \tilde{\lambda}_0^{\alpha} + \delta_1] \times \ldots \times [\tilde{\lambda}_{n_1+3}^{\alpha} - \delta_1, \tilde{\lambda}_{n_1+3}^{\alpha} + \delta_1]$ be the candidate set of $\boldsymbol{\lambda}_1$ in the objective function $f_1(\alpha, \tilde{\beta}_t^{\mathrm{I}_p}(\boldsymbol{\lambda}_1))$, where $\delta_1 > 0$ is a search window size. Instead of directly minimizing $f_1(\alpha, \tilde{\beta}_t^{\mathrm{I}_p}(\tilde{\boldsymbol{\lambda}}_1^{\alpha}))$ with respect to α, we consider profile minimization of $f_1(\alpha, \tilde{\beta}_t^{\mathrm{I}_p}(\boldsymbol{\lambda}_1))$ for $\boldsymbol{\lambda}_1 \in \Lambda_\alpha$ at each α, and then minimize over $\alpha \in \mathcal{A}$, where $\mathcal{A}$ is a candidate set for α. The profile optimization can lead to a better fitting of the objective function $f_1(\alpha, \tilde{\beta}_t^{\mathrm{I}_p}(\boldsymbol{\lambda}_1))$.

Given initial values $\hat{\mathcal{H}}^{\alpha}(t_1)$ at t_1, the candidate parameters α and $\beta_t^{\mathrm{I}_p}(\boldsymbol{\lambda}_1)$ with $\boldsymbol{\lambda}_1 \in \Lambda_\alpha$, and the estimated removal rates $\hat{\gamma}_{d,t}$ and $\hat{\gamma}_{r,t}$, we can simulate all nine states in the proposed vSVIADR model for $t \in \mathcal{S}_1$ based on (2) and (A.3), with $\{V_1(t), V_2(t), G_1(t), G_2(t)\}_{t\in\mathcal{S}_1}$ being set as zero for the pre-vaccine period. Let $\{I_p^{(b)}(t;\alpha,\boldsymbol{\lambda}_1,\hat{\mathcal{H}}^{\alpha}(t_1))\}_{t\in\mathcal{S}_1}$ be the bth simulated trajectory of the pre-symptomatic infections $I_p(t)$ over $\mathcal{S}_1$ for $b = 1, \ldots, B$ for a reasonably large integer B, which was set as 300 in the empirical analysis. All B trajectories are independently generated. We use the average simulated value $\tilde{I}_p(t;\alpha,\boldsymbol{\lambda}_1,\hat{\mathcal{H}}^{\alpha}(t_1)) = \sum_{b=1}^{B} I_p^{(b)}(t;\alpha,\boldsymbol{\lambda}_1,\hat{\mathcal{H}}^{\alpha}(t_1))/B$ to estimate $\mathrm{E}\{I_p(t)|\mathcal{F}_{t-1}\}$ given the candidate α and $\boldsymbol{\lambda}_1$. Then, the goodness-of-fit criterion function in (5) can be formulated by profiling out $\boldsymbol{\lambda}_1$ at a given α as

$$\tilde{f}_1(\alpha) = \min_{\boldsymbol{\lambda}_1\in\Lambda_\alpha} \frac{1}{|\mathcal{S}_1|} \sum_{t\in\mathcal{S}_1} \left\{ \tilde{I}_p(t;\alpha,\boldsymbol{\lambda}_1,\hat{\mathcal{H}}^{\alpha}(t_1))/\hat{I}_p^{\alpha}(t) - 1 \right\}^2. \tag{13}$$

The estimation of α is obtained by minimizing $\tilde{f}_1(\alpha)$ over $\mathcal{A}$ as

$$\hat{\alpha} = \underset{\mathcal{A}}{\operatorname{argmin}} \tilde{f}_1(\alpha). \tag{14}$$

Based on the clinical information (Guan et al., 2020), we chose $\mathcal{A} = [0.1, 0.2]$ implying the average diagnosis time is from 5 to 10 days before the start of public vaccination. By discretizing the search domain, the optimization problems (13) and (14) turn into the grid search in the space formed by $n_1 + 5$ parameters $\{\alpha, \lambda_{1,0}, \ldots, \lambda_{1,n_1+3}\}$. Other numerical algorithms, such as the genetic algorithm (Holland, 1992) may be applied to solve the optimization problems. We chose the grid search to ensure more accuracy. In the real data analysis, we set a grid resolution of 0.005 for the candidate set $\mathcal{A}$ of α, and chose the number of internal knots n_1 such that the maximum root mean squared relative error (RMSRE) $\max_{\alpha\in\mathcal{A}}[\sum_{t\in\mathcal{S}_1}\{\beta_t^{\mathrm{I}_p}(\tilde{\boldsymbol{\lambda}}_1^{\alpha})/\hat{\beta}_t^{\mathrm{I}_p,\alpha} - 1\}^2/(\#\{\mathcal{S}_1\})]^{1/2}$ of the regression (12) over $\alpha \in \mathcal{A}$ is less than 0.001 to guarantee enough basis functions to model the unknown infection rate function $\{\beta_t^{\mathrm{I}_p}\}_{t\in\mathcal{S}_1}$. The selected values of n_1 for the 10 countries are listed in Table S4 in the SM. Since the maximal coefficients of variation of the estimated coefficients $\{\tilde{\lambda}_k^{\alpha}\}_{k=0}^{n_1+3}$ from (12) for the 10 countries were less than 0.003, we set the search window δ_1 for the candidate set Λ_α to be 0.02 and a grid resolution of 0.01 for each component of Λ_α. Implemented in C++ using 100 cores on a server with Intel Xeon Gold 6132 2.6GHz CPUs, the time for calculating for $\hat{\alpha}$ for a country based on the average $\{\tilde{I}_p(t;\alpha,\boldsymbol{\lambda}_1,\hat{\mathcal{H}}^{\alpha}(t_1))\}_{t\in\mathcal{S}_1}$ of 300 trajectories for a 30-day time interval $\mathcal{S}_1$ was about 2 hours.

We chose $\mathcal{S}_1$ to be a 30-day period. The relatively short period permitted less number of spline basis functions to model $\beta_t^{\mathrm{I}_p}$ in order to save computational cost. From the regression estimation equation (10), larger $I_p(t)$ and $D(t)$ would make the estimate $\hat{\beta}_t^{\mathrm{I}_p,\alpha}$ more stable.

We intend to choose $\mathcal{S}_1$ around the peak $t_{\text{peak,1}} = \text{argmax}_{t\in\{1,\ldots,T_1\}} D(t)$ of $D(t)$ before T_1. Specifically, if $t_{\text{peak,1}} + 15 < T_1$, we set $\mathcal{S}_1 = \{t_{\text{peak,1}} - 15, \ldots, t_{\text{peak,1}} + 15\}$, otherwise, we set $\mathcal{S}_1 = \{T_1 - 31, \ldots, T_1 - 1\}$. As shown in Figure S2 in the SM, the peak infection times $t_{\text{peak,1}}$ of the 10 countries were within 55 days from T_1 except India and Peru, which were, respectively, 113 and 161 days ahead of their respective vaccine start date T_1.

4.3. *Estimation of vaccine effects φ and κ.* We consider data in a period $\mathcal{S}_2 = \{t_3, \ldots, t_4\} \subset \{T_1, \ldots, T_1 + l_1\}$ right after the start of vaccination to estimate the vaccine effect parameters φ and κ in the pre-Delta period. Similar to the objective function $f_1(\alpha, \beta_t^{\mathrm{I}_p})$ for estimating α in (5), we minimize the contrast measure

$$f_2(\varphi, \kappa, \beta_t^{\mathrm{I}_p}) = \frac{1}{|\mathcal{S}_2|} \sum_{t\in\mathcal{S}_2} \left\{ \hat{\mathrm{E}}^{\hat{\alpha},\varphi,\kappa}\{I_p(t)|\mathcal{F}_{t-1}\}/\hat{I}_p^{\hat{\alpha}}(t) - 1 \right\}^2, \tag{15}$$

where $\hat{I}_p^{\hat{\alpha}}(t) = \Delta N(t)/\hat{\alpha}$ is the imputed value of $I_p(t)$ by the estimated diagnosis rate $\hat{\alpha}$ obtained in (14), and $\hat{\mathrm{E}}^{\hat{\alpha},\varphi,\kappa}\{I_p(t)|\mathcal{F}_{t-1}\}$ is the simulation-based estimate of $\mathrm{E}\{I_p(t)|\mathcal{F}_{t-1}\}$ at given φ, κ and $\hat{\alpha}$ by averaging the simulated trajectories of the proposed Poisson-vSVIADR model, in the same way as the construction of $\tilde{I}_p(t; \alpha, \boldsymbol{\lambda}_1, \hat{\mathcal{H}}^{\alpha}(t_1))$ for the pre-vaccine period.

Let $\hat{\mathcal{H}}^{\hat{\alpha}}(T_1) = \{D(T_1), R_r(T_1), R_d(T_1), \hat{I}_p^{\hat{\alpha}}(T_1), \hat{I}_a^{\hat{\alpha}}(T_1), \hat{R}_a^{\hat{\alpha}}(T_1), \hat{S}^{\hat{\alpha}}(T_1), V_1(T_1), V_2(T_1)\}$ be the imputed state variables at time T_1, where $\hat{I}_p^{\hat{\alpha}}(T_1)$, $\hat{I}_a^{\hat{\alpha}}(T_1)$, $\hat{R}_a^{\hat{\alpha}}(T_1)$, $\hat{S}^{\hat{\alpha}}(T_1)$ are imputed by (5), (7) and (8) with the estimated diagnosis rate $\hat{\alpha}$, and $V_1(T_1) = V_2(T_1) = 0$. To obtain the trajectory of $I_p(t)$, similar as Section 4.2, we also use the B-spline model $\beta_t^{\mathrm{I}_p}(\boldsymbol{\lambda}_2) = \sum_{k=0}^{n_2+3} \lambda_{2,k}\psi_{k,4}\{(t - T_1)/l_1\}$ to approximate the infection rate $\beta_t^{\mathrm{I}_p}$ for $t \in \{T_1, \ldots, T_1 + l_1\}$ right after the start of vaccination, where n_2 is the number of internal knots and $\boldsymbol{\lambda}_2 = (\lambda_{2,0}, \ldots, \lambda_{2,n_2+3})$ is the coefficient vector. Then, the objective function in (15) becomes $f_2(\varphi, \kappa, \beta_t^{\mathrm{I}_p}(\boldsymbol{\lambda}_2))$.

Similar as the construction of the candidate set Λ_1 in Section 4.2, we obtain the candidate set of $\boldsymbol{\lambda}_2$ by considering two sets of regression $\{\hat{\beta}_t^{\mathrm{I}_p,\hat{\alpha}}\}_{t=T_1-l_1}^{T_1}$ before vaccination and $\{\hat{\beta}_{t,*}^{\mathrm{I}_p,\hat{\alpha}}\}_{t=T_1}^{T_1+l_1}$ after vaccination on the B-spline basis functions, and obtaining

$$\tilde{\boldsymbol{\lambda}}^{\text{before}} = (\tilde{\lambda}_0^{\text{before}}, \ldots, \tilde{\lambda}_{n_2+3}^{\text{before}}) = \underset{\boldsymbol{\lambda}_2}{\text{argmin}} \sum_{t=T_1-l_1}^{T_1} \left[\hat{\beta}_t^{\mathrm{I}_p,\hat{\alpha}} - \sum_{k=0}^{n_2+3} \lambda_{2,k}\psi_{k,4}\{(t - T_1 + l_1)/l_1\} \right]^2,$$

$$\tilde{\boldsymbol{\lambda}}^{\text{after}} = (\tilde{\lambda}_0^{\text{after}}, \ldots, \tilde{\lambda}_{n_2+3}^{\text{after}}) = \underset{\boldsymbol{\lambda}_2}{\text{argmin}} \sum_{t=T_1}^{T_1+l_1} \left[\hat{\beta}_{t,*}^{\mathrm{I}_p,\hat{\alpha}} - \sum_{k=0}^{n_2+3} \lambda_{2,k}\psi_{k,4}\{(t - T_1)/l_1\} \right]^2,$$

where $\{\hat{\beta}_t^{\mathrm{I}_p,\hat{\alpha}}\}_{t=T_1-l_1}^{T_1}$ is calculated from (11) with the estimated diagnosis rate $\hat{\alpha}$, and $\{\hat{\beta}_{t,*}^{\mathrm{I}_p,\hat{\alpha}}\}_{t=T_1}^{T_1+l_1}$ is calculated in the same way via updating the formulas leading to (11) for $t > T_1$. Note that $\{\hat{\beta}_{t,*}^{\mathrm{I}_p,\hat{\alpha}}\}_{t=T_1}^{T_1+l_1}$ is not a valid estimator for the infection rate $\{\beta_t^{\mathrm{I}_p}\}_{t=T_1}^{T_1+l_1}$ after the start of vaccination, as the estimator (11) is for the pre-vaccine stage without considering the vaccine effects. Our proposal here is to find a reasonable range of $\boldsymbol{\lambda}_2$ for minimizing $f_2(\varphi, \kappa, \beta_t^{\mathrm{I}_p}(\boldsymbol{\lambda}_2))$, and $\{\hat{\beta}_{t,*}^{\mathrm{I}_p,\hat{\alpha}}\}_{t=T_1}^{T_1+l_1}$ serve as a lower bound for $\{\beta_t^{\mathrm{I}_p}\}_{t=T_1}^{T_1+l_1}$ since the vaccine would have reduced the transmission resulting in a lowered than the should-be estimate of $\beta_t^{\mathrm{I}_p}$. In this sense, $\{\hat{\beta}_t^{\mathrm{I}_p,\hat{\alpha}}\}_{t=T_1-l_1}^{T_1}$ and $\{\hat{\beta}_{t,*}^{\mathrm{I}_p,\hat{\alpha}}\}_{t=T_1}^{T_1+l_1}$ provide approximate upper and lower bounds for $\{\beta_t^{\mathrm{I}_p}\}_{t=T_1}^{T_1+l_1}$, and the region between $\tilde{\boldsymbol{\lambda}}^{\text{before}}$ and $\tilde{\boldsymbol{\lambda}}^{\text{after}}$ should contain the true coefficient $\boldsymbol{\lambda}_2$. Like Λ_1, for a search window $\delta_2 > 0$, let Λ_2 be the cartesian product of $[\min(\tilde{\lambda}_i^{\text{before}}, \tilde{\lambda}_i^{\text{after}}) - \delta_2, \max(\tilde{\lambda}_i^{\text{before}}, \tilde{\lambda}_i^{\text{after}}) + \delta_2]$ for $i = 0, \ldots, n_2 + 3$. Similar as δ_1, we set δ_2 to 0.02 based on the variation of $\tilde{\lambda}_i^{\text{before}}$ and $\tilde{\lambda}_i^{\text{after}}$.

Let Θ be the candidate set of the vaccine parameters (φ, κ), which is set to $\{(\varphi, \kappa) : 0.5 \leq \varphi \leq 10, 0.01 \leq \kappa \leq 1, \varphi\kappa \leq 1\}$ based on the reported empirical VEs in recent studies summarized in Tables S1 and S2 in the SM. Then, the simulation of trajectories is generated from the proposed model system. Specifically, given the initial values $\hat{\mathcal{H}}^{\hat{\alpha}}(T_1)$ at time T_1, and the candidate model parameters $(\varphi, \kappa) \in \Theta$, $\beta_t^{\mathrm{I}_p}(\boldsymbol{\lambda}_2)$ with $\boldsymbol{\lambda}_2 \in \Lambda_2$ together with the estimated diagnosis rate $\hat{\alpha}$ and the estimated removal rates $\hat{\gamma}_{d,t}$ and $\hat{\gamma}_{r,t}$, we simulate all nine state variables for $t \in \{T_1, \ldots, T_1 + l_1\}$ according to the specification in (2) and (A.3). However, we do not generate $G_1(t)$ and $G_2(t)$ by the Poisson increments shown in (2) but directly use their observations, since they are irrelevant to the parameters of our interests, φ, κ and $\beta_t^{\mathrm{I}_p}$.

Let $\{I_p^{(b)}(t; \varphi, \kappa, \boldsymbol{\lambda}_2, \hat{\alpha}, \hat{\mathcal{H}}^{\hat{\alpha}}(T_1))\}_{t \in \mathcal{S}_2}$ be the bth simulated trajectory of the infected and pre-symptomatic cases over the target interval $\mathcal{S}_2$ for $b = 1, \ldots, B$, where B was 300 in the empirical analysis, and all the trajectories are independently generated. The average $\tilde{I}_p(t; \varphi, \kappa, \boldsymbol{\lambda}_2, \hat{\alpha}, \hat{\mathcal{H}}^{\hat{\alpha}}(T_1)) = \sum_{b=1}^{B} I_p^{(b)}(t; \varphi, \kappa, \boldsymbol{\lambda}_2, \hat{\alpha}, \hat{\mathcal{H}}^{\hat{\alpha}}(T_1))/B$ is used estimate $\mathrm{E}\{I_p(t)|\mathcal{F}_{t-1}\}$ after the start of vaccination at the candidate parameters φ, κ and $\boldsymbol{\lambda}_2$. Then, the criterion function (15) can be formulated by profiling out $\boldsymbol{\lambda}_2$ at the given φ and κ as

$$\tilde{f}_2(\varphi, \kappa) = \min_{\boldsymbol{\lambda}_2 \in \Lambda_2} \frac{1}{|\mathcal{S}_2|} \sum_{t \in \mathcal{S}_2} \{\tilde{I}_p(t; \varphi, \kappa, \boldsymbol{\lambda}_2, \hat{\alpha}, \hat{\mathcal{H}}^{\hat{\alpha}}(T_1))/\hat{I}_p^{\hat{\alpha}}(t) - 1\}^2, \tag{16}$$

and the estimator of (φ, κ) is

$$(\hat{\varphi}, \hat{\kappa}) = \underset{\Theta}{\operatorname{argmin}} \tilde{f}_2(\varphi, \kappa) \tag{17}$$

by conducting a grid search in the space formed by $n_2 + 6$ parameters $\{\varphi, \kappa, \lambda_{2,0}, \ldots, \lambda_{2,n_2+3}\}$.

In the real data analysis, we set $l_1 = 50$, and chose the number of internal knots n_2 such that the RMSREs of the B-spline fitting of $\boldsymbol{\lambda}_2$ are less than 0.005. The selected n_2 of the 10 countries for the pre-Delta, intervening and Delta dominated periods are listed in Table S4 in the SM. We set a grid resolution of 0.5×0.01 for Θ and 0.01 for each component $\lambda_{2,k}$ of Λ_2 in the grid search algorithm. The vaccine takes time to be effective. Usually, two weeks are required to form the protective effects against SARS-CoV-2 infections after receiving a dose. We chose a 30-day period 18 days after the start of the vaccination $\{T_1 + 18, \ldots, T_1 + 48\}$ as $\mathcal{S}_2$ in the estimation of the vaccine effect. The 18 days were slightly more than the 14 days recognised by the WHO for full vaccine effect, which was based on a slightly better performance in the simulation studies. The grid search algorithm used to optimize (17) to find $(\hat{\varphi}, \hat{\kappa})$ took about 8 hours for one country, which could be substantially reduced by applying the genetic algorithm.

The estimation of (φ, κ) in the intervening and the Delta dominated periods uses the same procedure as outlined above except that the starting date and the initial conditions need to be adjusted. The lengths of the target periods and the number of B-spline knots may be different to suit each period's situation.

4.4. *Estimation of infection rate* $\beta_t^{I_p}$. After having estimated the vaccine effects φ and κ and the diagnosis rate α, the estimates for infection rates in the pre-vaccine period $\{\hat{\beta}_t^{\mathrm{I}_p}\}_{t=1}^{T_1-1}$ are $\{\hat{\beta}_t^{\mathrm{I}_p, \hat{\alpha}}\}_{t=1}^{T_1-1}$ which are the estimator (11) at $\hat{\alpha}$, and we estimate the infection rate function $\beta_t^{\mathrm{I}_p}$ in the post-vaccine periods. We do not use the spline estimate for $\beta_t^{\mathrm{I}_p}$ used in Sections 4.2-4.3 since, after obtaining $\hat{\alpha}, \hat{\varphi}$ and $\hat{\kappa}$, a more tangible estimator based on the kernel regression estimator similar to (11) can be formulated in the post-vaccine era. However, we need to update the imputation by incorporating the vaccine compartments $V_1(t)$ and $V_2(t)$ to suit the post-vaccine situation as shown below.

From the conditional mean of $\Delta I_p(t)$ in (1), we have the approximation $\Delta I_p(t)+\alpha I_p(t) \approx \theta H(t,\boldsymbol{\beta}_t)\{S(t)+\varphi\kappa V_1(t)+\kappa V_2(t)\}$ similar to (10). Therefore, the conditional-mean-based imputation of $I_p(t)$, $I_a(t)$ and $R_a(t)$ via (5), (7) and (8) would remain the same, which is free of $V_1(t)$, $V_2(t)$, φ and κ regardless being before or after vaccination. Let $\hat{I}_p^{\hat{\alpha}}(t)$, $\hat{I}_a^{\hat{\alpha}}(t)$ and $\hat{R}_a^{\hat{\alpha}}(t)$ be such imputed values for $t > T_1$ with the estimated diagnosis rate $\hat{\alpha}$. To impute $V_1(t)$ and $V_2(t)$, note that $\{\Delta I_p(t)+\alpha I_p(t)\}/[\theta\{S(t)+\varphi\kappa V_1(t)+\kappa V_2(t)\}]$ can serve as a substitution for the total infection loading $H(t,\boldsymbol{\beta}_t)$. From Equation (A.3), we can impute $V_1(t)$ and $V_2(t)$ for $t > T_1$ by

$$\hat{V}_1^{\hat{\alpha}}(t+1) = (1-\mu_1)\hat{V}_1^{\hat{\alpha}}(t) + \Delta G_1(t) - \Delta G_2(t) - \frac{\hat{I}_p^{\hat{\alpha}}(t+1)-(1-\hat{\alpha})\hat{I}_p^{\hat{\alpha}}(t)}{\theta(\hat{S}^{\hat{\alpha}}(t)+\hat{\varphi}\hat{\kappa}\hat{V}_1^{\hat{\alpha}}(t)+\hat{\kappa}\hat{V}_2^{\hat{\alpha}}(t))}\hat{\varphi}\hat{\kappa}\hat{V}_1^{\hat{\alpha}}(t),$$

$$\hat{V}_2^{\hat{\alpha}}(t+1) = (1-\mu_2)\hat{V}_2^{\hat{\alpha}}(t) + \Delta G_2(t) - \frac{\hat{I}_p^{\hat{\alpha}}(t+1)-(1-\hat{\alpha})\hat{I}_p^{\hat{\alpha}}(t)}{\theta(\hat{S}^{\hat{\alpha}}(t)+\hat{\varphi}\hat{\kappa}\hat{V}_1^{\hat{\alpha}}(t)+\hat{\kappa}\hat{V}_2^{\hat{\alpha}}(t))}\hat{\kappa}\hat{V}_2^{\hat{\alpha}}(t),$$

with the initial values $V_1(T_1)=V_2(T_1)=0$. Then, $\hat{S}^{\hat{\alpha}}(t) = M - \hat{V}_1^{\hat{\alpha}}(t) - \hat{V}_2^{\hat{\alpha}}(t) - \hat{I}_a^{\alpha}(t) - \hat{I}_p^{\alpha}(t) - N(t) - \hat{R}_a^{\alpha}(t)$ is the imputed value of $S(t)$.

Similar to the kernel smoothing estimator in (11), we update the definitions of $Y(t)$ and $X(t)$ in the post-vaccine period ($t > T_1$) as $Y(t) = \{\hat{I}_p^{\hat{\alpha}}(t+1)+(\hat{\alpha}-1)\hat{I}_p^{\hat{\alpha}}(t)\}/\theta$ and

$$X(t) = \left[\hat{I}_p^{\hat{\alpha}}(t) + \{D(t)+\hat{I}_a^{\hat{\alpha}}(t)\}/r\right]\left\{\hat{S}^{\hat{\alpha}}(t)+\hat{\varphi}\hat{\kappa}\hat{V}_1^{\hat{\alpha}}(t)+\hat{\kappa}\hat{V}_2^{\hat{\alpha}}(t)\right\}/M,$$

where $Y(t)$ still approximates the total number of the newly infected at t and $\beta_t^{\mathrm{I}_p}X(t)$ approximates its expected value in the post-vaccine period. Therefore, the time varying infection rate $\beta_t^{\mathrm{I}_p}$ can be estimated by the locally weighted kernel regression of $Y(t)$ on $X(t)$ under the imputed values of the unobserved state variables. For $t = T_1+1,\ldots,T-2$,

$$\begin{aligned}\hat{\beta}_t^{\mathrm{I}_p} &= \arg\min_{\beta} \sum_{i=T_1+1}^{T-2} \{Y(i)-X(i)\beta\}^2 B\left(\frac{t-i}{h}\right) \\ &= \frac{\sum_{i=T_1+1}^{T-2} X(i)Y(i)B\{(t-i)/h\}}{\sum_{i=T_1+1}^{T-2} X(i)^2 B\{(t-i)/h\}}. \end{aligned} \tag{18}$$

The regression use $Y(t)$ and $X(t)$ until $T-2$ since the imputed values $\hat{I}_p^{\hat{\alpha}}(t+1) = \Delta N(t+1)/\hat{\alpha}$ used in $Y(t)$ can only be obtained for $t \le T-2$. Note that the estimator $\hat{\beta}_t^{\mathrm{I}_p,\hat{\alpha}}$ in (11) for the infection rates in the pre-vaccine period is a special case of (18) with $\hat{V}_1^{\hat{\alpha}}(t)$ and $\hat{V}_2^{\hat{\alpha}}(t)$ set to zero for $t \in \{1,\ldots,T_1\}$. The estimation procedure of $\beta_t^{\mathrm{I}_p}$ in the intervening and Delta dominated period is the same except using each period's $\hat{\varphi}$ and $\hat{\kappa}$.

4.5. *Parametric bootstrap inference.* Let $\boldsymbol{\eta} = \{\alpha, (\varphi_i,\kappa_i)_{i=1}^3, (\beta_t^{\mathrm{I}_p},\gamma_{r,t},\gamma_{d,t})_{t=1}^T\}$ be the epidemiological parameters of our concern in the whole study period, where $\{(\varphi_i,\kappa_i)\}_{i=1}^3$ are the vaccine effect parameters for the pre-Delta, intervening and Delta dominated period, respectively. And we denote the generation process by our proposed SEM based on (2) and (A.3) at the given $\boldsymbol{\eta}$ as vSVIADR($\boldsymbol{\eta}$). To obtain an uncertainty measure for these epidemiological parameters, we consider using the parametric bootstrap procedure under the vSVIADR($\hat{\boldsymbol{\eta}}$) model with the estimated parameters $\hat{\boldsymbol{\eta}}$.

Specifically, let $\{S^*(t), V_1^*(t), V_2^*(t), I_a^*(t), I_p^*(t), D^*(t), R_a^*(t), R_r^*(t), R_d^*(t)\}_{t=1}^T$ be a resampled trajectory of the entire state variables from the bootstrap. Given $\hat{\alpha}$, $\hat{\beta}_t^{\mathrm{I}_p}$, $\hat{\gamma}_{r,t}$, $\hat{\gamma}_{d,t}$, and the observed and imputed initial values $\{D(1), R_r(1), R_d(1), \hat{I}_a^{\hat{\alpha}}(1), \hat{I}_p^{\hat{\alpha}}(1), \hat{R}_a^{\hat{\alpha}}(1), \hat{S}_a^{\hat{\alpha}}(1)\}$,

bootstrap resampled trajectories for the first T_1 days in the pre-vaccine period were generated by substituting these estimates into (2) and (A.3) with setting $\{V_1^*(t), V_2^*(t), G_1^*(t), G_2^*(t)\}_{t=1}^{T_1}$ to zero. Then, the bootstrap resampling for the pre-Delta period was conducted via vSVIADR($\hat{\boldsymbol{\eta}}$) with the initial value $\{S^*(T_1),\ V_1^*(T_1),\ V_2^*(T_1),\ I_a^*(T_1),\ I_p^*(T_1),\ D^*(T_1),\ R_a^*(T_1),\ R_r^*(T_1),\ R_d^*(T_1)\}$ according to (2) and (A.3). For the resampling in this period, we did not resample $G_1(t)$ and $G_2(t)$ but used their original observations since they are irrelevant to $\boldsymbol{\eta}$ which can be seen in (2). The following bootstrap resampled data in the intervening and Delta dominated period can be generated in the same way with the estimates for the corresponding estimated parameters in $\hat{\boldsymbol{\eta}}$.

The parameter $\boldsymbol{\eta}$ was re-estimated based on the bootstrap resampled observations. The resampling was replicated for a large number (B) of times to obtain B independent bootstrap estimates $\{\hat{\boldsymbol{\eta}}^{b,*}\}_{b=1}^{B}$ for the parameter. The sample standard deviation of the bootstrap estimates can be used to estimate the standard error of $\hat{\boldsymbol{\eta}}$. Let $\hat{\eta}^*_{i(0.025)}$ and $\hat{\eta}^*_{i(0.975)}$ be, respectively, the 2.5th and 97.5th percentile of the bootstrap estimates for η_i, the ith element of $\boldsymbol{\eta}$. Then, the 95% bootstrap confidence interval of η_i is $[\hat{\eta}^*_{i(0.025)}, \hat{\eta}^*_{i(0.975)}]$.

5. Simulation experiments. To illustrate the performance of the proposed estimation method and the asymptotic performance of the estimators as the population size M increases, we designed a simulation in which the length of data before and after the start of vaccination was $T_1 = 300$ and $T_2 = 50$ days, respectively. To mimic the COVID-19 reality, we set $r = 5$, $\alpha = 0.15$, $\mu_1 = 1/60$, $\mu_2 = 1/240$, $\theta = 0.8$, $(\varphi, \kappa) \in \{(2.5, 0.1), (1.5, 0.4)\}$, $M \in \{5 \times 10^8, 1 \times 10^9, 1.5 \times 10^9\}$, $I_a(1)/M = 5 \times 10^{-8}$, $I_p(1)/M = 2 \times 10^{-7}$, $D(1)/M = 3 \times 10^{-8}$, $R_r(1)/M = 4 \times 10^{-8}$, $R_a(1) = R_d(1) = G_1(1) = G_2(1) = 0$, $\phi_{1,t} = 0.005 \times \mathbf{1}_{(T_1,T_2]}(t)$ and $\phi_{2,t} = 0.025 \times \mathbf{1}_{(T_1,T_2]}(t)$, where $\mathbf{1}_A(t)$ is the indicator function with value 1 if $t \in A$, and 0 otherwise. For the varying coefficient parameters, to make the simulation in line with the data in real-world situations, we mimicked the pattern of the estimated infection, recovery and death rates of the US in the pre-vaccine period. Specifically, we set the recovery rate $\gamma_{r,t} = 0.07$ over the whole period, $\gamma_{d,t} = \{0.01 + \frac{0.0088}{129}(1 - t)\}\mathbf{1}_{[1,131)}(t) + 0.00119 \times \mathbf{1}_{[131,T_1+T_2]}(t)$ for the death rate, which linearly decreases in the first 130 days and then remains constant, and $\beta_t^{\mathrm{I}_p} = [-0.4 + \exp\{0.014(1-t)\}]\mathbf{1}_{[1,50]}(t) + \{0.1 + \frac{0.078}{70}(t-50)\}\mathbf{1}_{(50,120]}(t) + \{0.178 - \frac{0.043}{80}(t-120)\}\mathbf{1}_{(120,200]}(t) + \{0.135 + \frac{0.005}{20}(t-200)\}\mathbf{1}_{(200,220]}(t) + 0.14 \times \mathbf{1}_{(220,T_1]}(t)$ for the pre-vaccine period $t \le T_1$, which consists of segments of exponential decrease, linear increase, linear decrease and constant functions. See Figure S3 in the SM for the comparison of the piece-wise curves in our setting with those of the US estimates.

For each combination of the parameter settings, we considered three different settings of the infection rate after the vaccination: (i) constant trend $\beta_t^{\mathrm{I}_p} \equiv 0.14$; (ii) increasing trend $\beta_t^{\mathrm{I}_p} = 0.14 + 8 \times 10^{-8}(t - T_1)^3$; and (iii) decreasing trend $\beta_t^{\mathrm{I}_p} = 0.14 - 8 \times 10^{-8}(t - T_1)^3$. For each parameter setting, the trajectories of all compartments were generated by adding up the Poisson increments over time according to (2) and (A.3), and this process was independently repeated 100 times. For each repetition, we use the estimation method described in Section 4 to obtain $\hat{\alpha}$, $\hat{\varphi}$ and $\hat{\kappa}$ by (14) and (17), and then the infection rate by (18).

Table 1 reports the estimation results for α and the vaccine effects $(1 - \varphi\kappa, 1 - \kappa)$ for the partial and fully vaccinated group, which are equal to $(0.75, 0.9)$ and $(0.4, 0.6)$ under the settings of $(\varphi, \kappa) = (2.5, 0.1)$ and $(\varphi, \kappa) = (1.5, 0.4)$, respectively. Figures 2 and S4-S8 in the SM display the estimation results of the time-varying coefficients $\beta_t^{\mathrm{I}_p}$, $\gamma_{d,t}$, $\gamma_{r,t}$ and R_t, with the comparison to their true values. These results reveal general satisfactory performance of the estimation procedure. For each setting of parameters, the standard errors of the estimates over 100 replications decreased with the increase of the population size. Generally, the bias

TABLE 1

Average estimates ($10^3\times$ the standard errors) of the diagnosis rate α, the vaccine efficacy $1-\varphi\kappa$ and $1-\kappa$ for the partial and full vaccination respectively, under different parameter settings based on 100 simulations.

$(\alpha, 1-\varphi\kappa, 1-\kappa)$	$\beta_t^{\mathrm{I}_p}$	Population size	$\hat{\alpha}$	$1-\hat{\varphi}\hat{\kappa}$	$1-\hat{\kappa}$
(0.15, 0.75, 0.9)	Constant	5×10^8	0.151 (1.2)	0.754 (4.6)	0.894 (2.8)
		1×10^9	0.150 (0.9)	0.757 (3.7)	0.893 (2.3)
		1.5×10^9	0.150 (0.5)	0.753 (2.2)	0.898 (2.2)
	Increasing	5×10^8	0.150 (1.5)	0.753 (5.9)	0.898 (2.8)
		1×10^9	0.150 (0.7)	0.749 (3.1)	0.899 (2.7)
		1.5×10^9	0.150 (0.4)	0.746 (1.9)	0.908 (2.1)
	Decreasing	5×10^8	0.155 (1.6)	0.741 (6.1)	0.892 (2.9)
		1×10^9	0.152 (1.2)	0.746 (4.5)	0.894 (2.4)
		1.5×10^9	0.151 (0.6)	0.755 (2.5)	0.885 (1.9)
(0.15, 0.4, 0.6)	Constant	5×10^8	0.149 (1.4)	0.402 (4.3)	0.615 (3.4)
		1×10^9	0.151 (0.9)	0.396 (2.2)	0.604 (2.0)
		1.5×10^9	0.150 (0.5)	0.401 (1.2)	0.601 (0.8)
	Increasing	5×10^8	0.152 (1.5)	0.393 (3.8)	0.612 (2.8)
		1×10^9	0.151 (1.1)	0.396 (2.7)	0.605 (2.0)
		1.5×10^9	0.151 (0.7)	0.398 (1.6)	0.601 (1.3)
	Decreasing	5×10^8	0.153 (1.6)	0.392 (4.4)	0.611 (3.5)
		1×10^9	0.151 (0.9)	0.398 (2.3)	0.605 (2.0)
		1.5×10^9	0.150 (0.6)	0.400 (1.5)	0.601 (0.9)

of the estimates also decreased as the population size increased, which was obvious under the setting $(1-\varphi\kappa, 1-\kappa) = (0.4, 0.6)$ due to more vaccinated people being infected. From Figure 2, the differences between the estimates $\hat{\gamma}_{d,t}$ and $\hat{\gamma}_{r,t}$ and their true values suggest that their variation decreased with time t due to the increasing number of infected people (sample size). There was no obvious trend in the variations of $\hat{\beta}_t^{\mathrm{I}_p}$ and $\hat{R}_t$ over time since our multi-step decentralized estimation made the variation of these estimates be also influenced by the variation of the other parameters, including $\hat{\alpha}$, $\hat{\gamma}_{d,t}$, $\hat{\gamma}_{r,t}$, $\hat{\varphi}$ and $\hat{\kappa}$.

6. Results on vaccine efficacy. We applied the proposed SEM and the inference procedures presented in Section 4 to evaluate the real-world VEs in the ten countries, which are represented by $1-\varphi\kappa$ and $1-\kappa$ for the partial and full vaccination under our model, respectively. We estimated the VEs in the three periods (the pre-Delta, intervening and Delta dominated) after vaccination for the ten countries. The results are reported in Table 2. India did not have the pre-Delta period after vaccination as stated in Section 2. It is noted that the VE estimated in the Delta period was not against the Delta variant only, but against all strains that occurred in this period.

Table 2 shows that the overall VEs of the full vaccination during the pre-Delta period in the 9 countries without India were 68%-95% (Average: 81%, SE: 4%) while those of the partial vaccination were 48%-64% (Average: 56%, SE: 2%), which suggested that the full vaccination would bring 12%-40% (Average:24%, SE: 4%) more VE than the partial vaccination. Hence, the full vaccination's VEs regardless of the brands and their combinations all passed the 50% threshold for being effective according to the WHO guideline (WHO, 2021), while the partial vaccination's VEs largely passed the threshold except Turkey whose was at 48%.

The full vaccination's VEs of the countries in the intervening period were 49%-87% (Average: 69%, SE 3%) and those of the partial vaccination were 23.5%-67.5% (Average: 47%, SE 4%), which were both significantly lower than those in the pre-Delta period. However, the full vaccination still offered 15%-33% (Average 22%, SE 2%) more protection than the partial one.

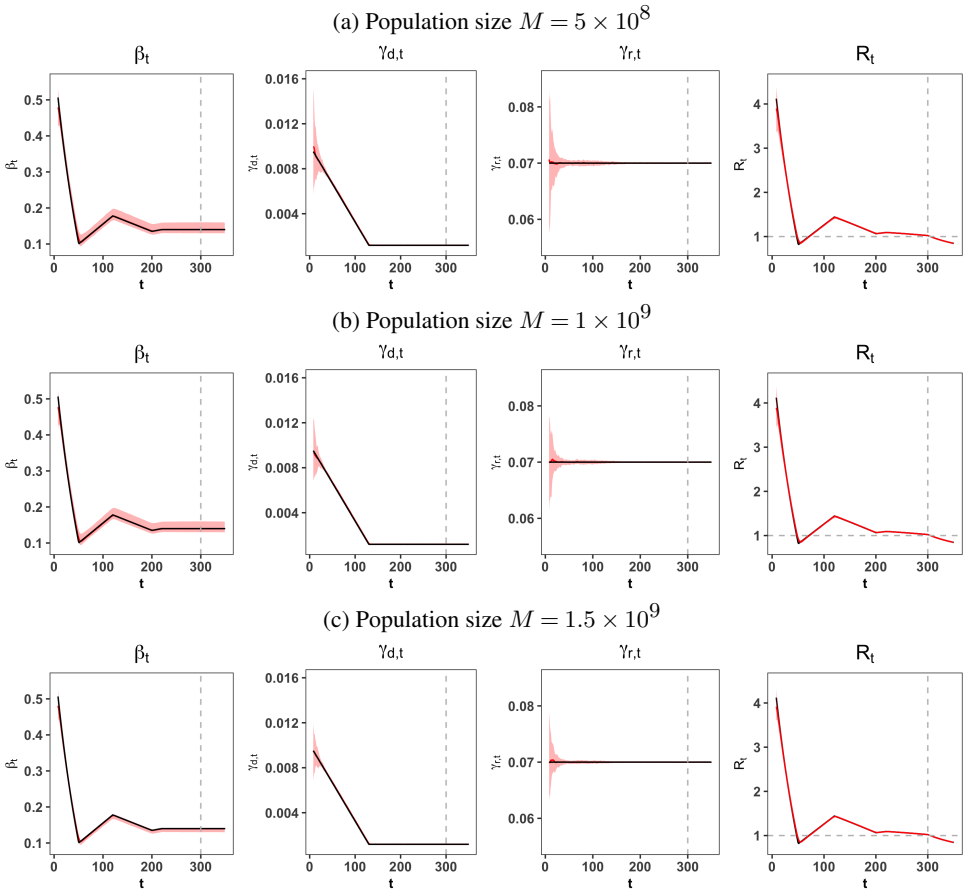

Fig 2: Curves of true (black) and estimated (red) $\beta_t^{\mathrm{I}_p}, \gamma_{r,t}, \gamma_{d,t}$ and R_t with the colored 2.5%-97.5% quantile bands for three population sizes. The dashed vertical line marks the start of vaccination. The true values of infection rates after the start of the vaccination were 0.14, and α, φ and κ were 0.15, 2.5 and 0.1, respectively.

When the Delta variant was prevalent, the partial vaccination showed even lower VEs ranging from 17.5% to 48% (Average: 35%, SE 3%). Only the US's and Peru's partial VEs stayed above 40%. Thus, the partial vaccination was not sufficiently protective against the Delta strain in the ten countries, which was consistent with the findings in Li et al. (2021) based on a small size retrospective study and Planas et al. (2021) via investigating the neutralising capacity of sera from vaccine recipients. The VEs of the full vaccination during the Delta period were 45%-74% (Average: 59%, SE: 2%), with the highest being 74% (CI: 69% to 79%) in the US and the lowest 45% (CI: 40% to 50%) in Turkey. The full vaccination during the Delta period had 19.5%-36% (average 24%, SE 2%) premium beyond the partial vaccination, indicating the boosting effect of the full vaccination against the Delta variant.

Table 2 indicates waning VEs as the Delta variant gradually became the dominant strain, whether for partial or full vaccination. Compared to the pre-Delta period, the VEs of full vaccination in the Delta dominated period for the 9 countries without India decreased by 10%-37% (average 21%, SE 3%), while those for partial vaccination decreased by 7%-30.5% (average 21%, SE 2%). Relative to the intervening period, the VEs of full vaccination in the Delta dominated period were reduced by 4%-14% (average 10%, SE 1%), and those of the partial vaccination by 1%-19.5% (average 12%, 2%). The average effectiveness of partial vaccination in the three periods was 23% (SE: 1%) less than that of the full vaccination, which

was consistent with the findings in a test-negative case-control study in England (Bernal et al., 2021) and also the sera neutralising capacity study in Planas et al. (2021).

Most of the ten countries used a mixed brand of vaccines. Our results suggested that the estimated VEs were similar among countries administrated with the same type of vaccines in a period. For example, the estimated VEs in Germany and Italy were close over the three periods for both partial and full vaccination. In addition to vaccine types, the VEs were also affected by the distribution strategy of different vaccines, and the SARS-Cov-2 variants in a country. Although we did not have access to these information, we will provide results on a distribution scenario with regards to the first dose of vaccine in the next section.

Over the three periods, the US had the highest VEs among the 10 countries, where two RNA-based vaccines Moderna and Pfizer were applied. Turkey where an inactivated vaccine was administrated had the lowest VEs in the intervening and Delta dominated period. These results were supported by two comprehensive analyses (Cai et al., 2021a,b) on the efficacy of COVID-19 vaccines using the published test-negative designs and clinical trials, which found RNA-based vaccines' VE ranked first, followed by the viral vector vaccines and then the inactivated vaccines.

7. Scenario analysis. To evaluate community transmission of COVID-19 in the ten countries, we estimate the effective reproduction number R_t via (3) under the vSVIADR model. The estimated R_t curves are displayed in Figure 3 (a), which shows a strong correlation between $R_t > 1$ and the substantial increase of the newly confirmed cases $\Delta N(t)$. Figure 3 (b) shows that the estimated R_t was highly correlated with the estimated infection rates $\beta_t^{\mathbf{I}_p}$, with the generally higher infection rates in the Delta dominated period as compared to the pre-Delta and intervening periods. For many countries, R_t gradually dropped below 1 after vaccination in the pre-Delta period, but rose above 1 as the Delta variant became prevalent.

TABLE 2

The estimated diagnosis rates, and efficacy of the partial and full vaccination in the pre-Delta, the intervening and the Delta dominated periods for the 10 countries. The standard errors obtained by the bootstrap method are reported in the parentheses.

Country	Diagnosis rate	Period	Time range	Vaccine	Partial vaccination	Full vaccination
Brazil	0.115 (0.014)	Pre-Delta	2021-01-16 ∼ 2021-05-19	AstraZeneca, Sinovac	0.625 (0.07)	0.75 (0.03)
		Intervening	2021-05-20 ∼ 2021-08-15	Pfizer, AstraZeneca, Sinovac	0.52 (0.05)	0.68 (0.03)
		Delta dominated	2021-08-16 ∼ 2021-11-20	Janssen, Pfizer, AstraZeneca, Sinovac	0.385 (0.05)	0.59 (0.03)
Canada	0.110 (0.010)	Pre-Delta	2020-12-13 ∼ 2021-03-14	Moderna, AstraZeneca, Pfizer	0.58 (0.07)	0.86 (0.02)
		Intervening	2021-03-15 ∼ 2021-07-04	Moderna, AstraZeneca, Pfizer	0.45 (0.05)	0.78 (0.03)
		Delta dominated	2021-07-05 ∼ 2021-11-20	Moderna, AstraZeneca, Pfizer	0.28 (0.05)	0.64 (0.03)
Germany	0.120 (0.012)	Pre-Delta	2020-12-26 ∼ 2021-02-28	Janssen, Moderna, AstraZeneca, Pfizer	0.56 (0.07)	0.89 (0.02)
		Intervening	2021-03-01 ∼ 2021-07-04	Janssen, Moderna, AstraZeneca, Pfizer	0.505 (0.05)	0.67 (0.03)
		Delta dominated	2021-07-05 ∼ 2021-11-20	Janssen, Moderna, AstraZeneca, Pfizer	0.40 (0.04)	0.60 (0.03)
India	0.100 (0.008)	Intervening	2021-01-15 ∼ 2021-04-11	Covaxin, AstraZeneca	0.46 (0.05)	0.64 (0.04)
		Delta dominated	2021-04-12 ∼ 2021-11-20	Covaxin, AstraZeneca	0.325 (0.05)	0.55 (0.03)
Italy	0.200 (0.007)	Pre-Delta	2020-12-26 ∼ 2021-04-01	Janssen, Moderna, AstraZeneca, Pfizer	0.58 (0.07)	0.94 (0.01)
		Intervening	2021-04-02 ∼ 2021-07-04	Janssen, Moderna, AstraZeneca, Pfizer	0.55 (0.05)	0.7 (0.02)
		Delta dominated	2021-07-05 ∼ 2021-11-20	Janssen, Moderna, AstraZeneca, Pfizer	0.355 (0.02)	0.57 (0.01)
Peru	0.110 (0.011)	Pre-Delta	2021-02-07 ∼ 2021-06-09	AstraZeneca, Pfizer, Sinopharm	0.64 (0.06)	0.76 (0.04)
		Intervening	2021-06-10 ∼ 2021-09-12	AstraZeneca, Pfizer, Sinopharm	0.46 (0.06)	0.73 (0.04)
		Delta dominated	2021-09-13 ∼ 2021-11-20	AstraZeneca, Pfizer, Sinopharm	0.415 (0.04)	0.61 (0.03)
Portugal	0.160 (0.012)	Pre-Delta	2020-12-26 ∼ 2021-04-04	Moderna, AstraZeneca, Pfizer	0.52 (0.06)	0.68 (0.04)
		Intervening	2021-04-05 ∼ 2021-05-23	Janssen, Moderna, AstraZeneca, Pfizer	0.38 (0.06)	0.69 (0.03)
		Delta dominated	2021-05-24 ∼ 2021-11-20	Janssen, Moderna, AstraZeneca, Pfizer	0.37 (0.05)	0.58 (0.03)
Turkey	0.160 (0.011)	Pre-Delta	2021-02-11 ∼ 2021-04-27	Sinovac, Pfizer	0.48 (0.05)	0.74 (0.04)
		Intervening	2021-04-28 ∼ 2021-06-20	Sinovac, Pfizer	0.235 (0.05)	0.49 (0.03)
		Delta dominated	2021-06-21 ∼ 2021-11-20	Sinovac, Pfizer	0.175 (0.04)	0.45 (0.03)
UK	0.140 (0.013)	Pre-Delta	2021-01-09 ∼ 2021-02-21	AstraZeneca, Pfizer	0.52 (0.04)	0.68 (0.03)
		Intervening	2021-02-22 ∼ 2021-05-23	Moderna, AstraZeneca, Pfizer	0.46 (0.06)	0.64 (0.04)
		Delta dominated	2021-05-24 ∼ 2021-11-20	Moderna, AstraZeneca, Pfizer	0.34 (0.05)	0.56 (0.03)
US	0.100 (0.003)	Pre-Delta	2020-12-12 ∼ 2021-02-22	Moderna, Pfizer	0.55 (0.07)	0.95 (0.01)
		Intervening	2021-02-23 ∼ 2021-06-20	Janssen, Moderna, Pfizer	0.675 (0.05)	0.87 (0.02)
		Delta dominated	2021-06-21 ∼ 2021-11-20	Janssen, Moderna, Pfizer	0.48 (0.05)	0.74 (0.03)

(a) The scaled $\Delta N(t)$, $\Delta R_d(t)$ and the estimated R_t

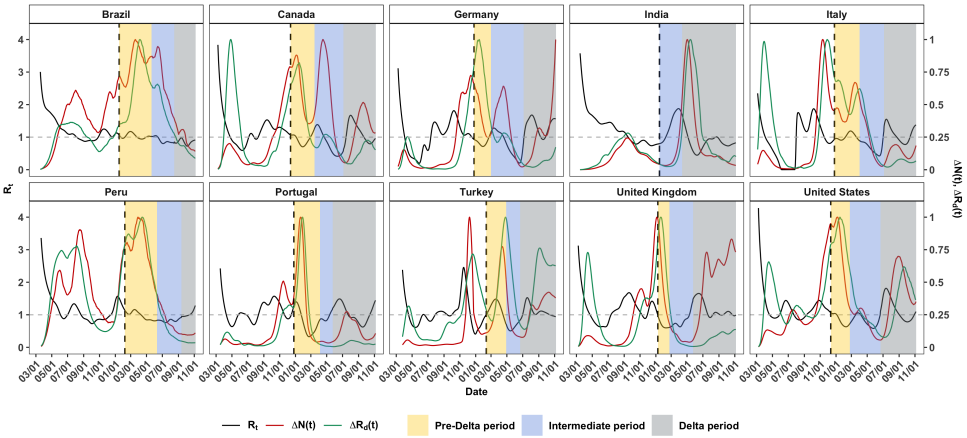

(b) The estimated $\beta_t^{\mathrm{I}_p}$, and the empirical and would-be R_t

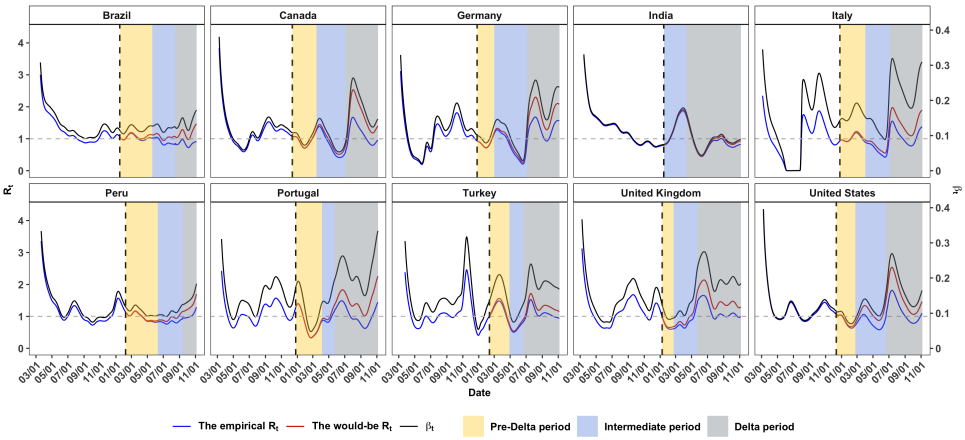

Fig 3: (a) Estimated R_t (black), and the daily increase of confirmed cases $\Delta N(t)$ (red) and death $\Delta R_d(t)$ (green) rescaled to $[0, 1]$ by their respective maximums from March 5, 2020 to November 5, 2021. (b) Estimates of the infection rates $\beta_t^{\mathrm{I}_p}$, the empirical (blue) and the would-be (red) R_t. The yellow, light blue and gray colored areas mark the pre-Delta, intervening and Delta periods, respectively. The dashed vertical lines indicate the vaccination start dates.

The effective reproduction number without vaccines is $\big\{(1-\theta)\beta_t^{\mathrm{I}_a}/\gamma_{r,t} + \theta\big(\beta_t^{\mathrm{I}_p}/\alpha + \beta_t^{\mathrm{D}}/\gamma_t\big)\big\}\{S(t) + V_1(t) + V_2(t)\}/M$. Figure 3 (b) shows that the would-be R_t curves were higher than those of the empirically observed R_t defined in (3) after the start of vaccination, especially when the Delta variant was dominated. This suggests that vaccines contributed to reducing the effective reproduction number R_t substantially in the Delta dominated period. The average empirically observed R_t in the post-vaccine period for the 10 countries was 20% less than that of the would-be R_t without vaccination.

Another way to evaluate the vaccine effects is to calculate the would-be confirmed cases and deaths under no vaccination at all and the partial vaccination only without going for the full vaccination. For each country, the two scenarios were created by dynamically generating the nine states from the proposed vSVIADR model under each scenario. Since the vaccine effects are accounted by $\{(\varphi_i, \kappa_i)\}_{i=1}^3$, we used the empirically estimated diagnosis rate $\hat{\alpha}$, the infection rates $\hat{\beta}_t^{\mathrm{I}_p}$, the recovery rates $\hat{\gamma}_{r,t}$ and the death rates $\hat{\gamma}_{d,t}$ shown in Table 2, and

TABLE 3

The increases (the 95% confidence intervals) and the percentages of increase in the confirmed cases and deaths on October 31, 2021 for the 10 countries under the no (No), partial (Part) and first-dose-priority (First) vaccination scenarios.

Country	Confirmed cases (thousand)				Death (thousand)			
	Increase (95% CI)	Percentage %			Increase (95% CI)	Percentage %		
	No	No	Part	First	No	No	Part	First
Brazil	14915.6 (14801.6, 15040.1)	68	13	0	312.4 (308.4, 315.7)	51	9	0
Canada	13265.8 (13141.7, 13422.1)	769	411	77	109.2 (107.7, 110.9)	376	188	34
Germany	21600.6 (21363.6, 21833.3)	465	188	36	104.5 (102.6, 106.1)	109	37	5
India	6184.0 (5829.7, 6534.8)	18	6	4	75.3 (70.2, 79.8)	16	6	3
Italy	10817744 (10683.9, 10954.7)	227	61	7	95.4 (93.7, 97.0)	72	17	0
Peru	276.9 (255.3, 295.6)	13	4	0	10.9 (9.6, 12.2)	5	2	0
Portugal	2654.8 (2599.0, 2713.4)	243	88	51	13.0 (12.6, 13.4)	72	24	11
Turkey	10647.1 (10521.0, 10724.6)	132	74	34	76.1 (75.1, 77.0)	108	57	26
UK	25284.4 (25214.1, 25349.7)	278	214	134	74.7 (74.1, 75.4)	53	44	25
US	153210.8 (153132.6, 153294.3)	333	232	98	1688.6 (1686.1, 1691.8)	226	166	70
Total	258857.7 (257542.3, 260162.9)	194	117	49	2560.1 (2540.1, 2579.3)	102	62	24

Figures 3 (b) and S9. We set $\{(\varphi_i, \kappa_i)\}_{i=1}^3$ and $\{V_1(t), V_2(t), G_1(t), G_2(t)\}_{t=T_1}^T$ to zero for the no-vaccination scenario, used the observed $\{G_1(t)\}_{t=T_1}^T$ and the estimates $\{(\hat{\varphi}_i, \hat{\kappa}_i)\}_{i=1}^3$ as well as making $\{V_2(t), G_2(t)\}_{t=T_1}^T$ to zero for the partial-vaccination scenario. We also designed a first-dose-priority vaccination scenario which gave priority to the first dose, and then the second dose if there were remaining vaccines left for it. This design can be realized by using the estimates $\{(\hat{\varphi}_i, \hat{\kappa}_i)\}_{i=1}^3$ and changing the vaccination functions $\{G_1(t)\}_{t=T_1}^T$ to $\{\min\{G_1(t)+G_2(t), M\}\}_{t=T_1}^T$ and $\{G_2(t)\}_{t=T_1}^T$ to $\{\max\{G_1(t)+G_2(t)-M, 0\}\}_{t=T_1}^T$. The simulated trajectories under the three scenarios were made based on (2) and (A.3) with the initial values $\{\hat{S}^{\hat{\alpha}}(T_1), V_1(T_1), V_2(T_1), \hat{I}_a^{\hat{\alpha}}(T_1), \hat{I}_p^{\hat{\alpha}}(T_1), \hat{R}_a^{\hat{\alpha}}(T_1), D(T_1), R_r(T_1), R_d(T_1)\}$. And the simulations of the three scenarios were repeated 100 times for each country under each scenario.

Table 3 provides the would-be increases in confirmed cases and deaths under the no-vaccine, partial-vaccine and first-dose-priority scenarios relative to the observed values. Comparing to the observations up to October 31, 2021, there would be 259 million increase in confirmed cases and 2.6 million increase in deaths for the 10 countries combined in the absence of vaccination, which would amount to 194% and 102% increase over the observed confirmed cases and deaths, respectively. Under the partial-vaccination scenario, there would be 117% and 62% increases in confirmed cases and deaths, respectively. The first-dose-priority scenario would lead to the respective increases of 49% and 24% in the total confirmed cases and deaths, indicating it would not be a better strategy than the existing one used by the countries, although the increases in Brazil, Italy and Peru were not significant. The details on the number of the would-be increases are reported in Table S5 in the SM. The increase in the cases and deaths would have been particularly phenomenal for Canada, Germany and the USA, with 333-769% increases in confirmed cases and 109-376% increases in deaths under the no-vaccine scenario. In a sharp contrast, the would-be increases in both the cases and deaths in India and Peru were rather small. These were due to, as shown in Figure S10, the much lower vaccination rates in Peru (46%) and India (23%), as compared with the other countries.

The actual and the average would-be confirmed cases and deaths generated under the three scenarios are displayed in Figure S11 in the SM, which shows that the gaps between the would-be and the observed grew with respect to time for most countries and scenarios especially in the Delta dominated period due to the higher would-be R_t in almost all countries. These are another reflection on the vaccines' effect in reducing the epidemics.

8. Conclusion. This paper proposes a stochastic epidemiological model and an estimation procedure to evaluate vaccine efficacy against COVID-19 infection based on publicly

available data. The real-world evaluation of vaccine efficacy is operated under stochasticity, non-permanent immunity and breakthrough infections which were not considered in Dashtbali and Mirzaie (2021) and Giordano et al. (2021). The proposed decentralized estimation needs to obtain values of some model parameters based on published external studies due to some state variables are latent. However, some of these parameters may be incorporated into the proposed estimation framework, for instance, the coefficient r among the three infection rates may be estimated by enlarging the model-based simulation. Further studies are needed in this regard. It is also noted that the imputation of various compartments is based on the mean specification of Model (2).

The Poisson regression in (2) implicitly assumes the means of the daily increments are equal to their variances. If overdispersion exists in the observed data, negative binomial regression with the same mean specification can be used to replace the Poisson assumption in (2). Given the mean μ_t, the variance of the negative binomial distribution is equal to $\mu_t + \mu_t^2/\varpi$ for an overdispersion parameter ϖ. A similar estimation procedure can be carried out to estimate the model parameters by including the additional parameter ϖ in the objective functions (5) and (15), and simulating the trajectories of the proposed model under the negative binomial distribution.

Our analyses on the 10 countries' data show significant real-world vaccine benefits in slowing down the COVID-19 infection, largely meeting the WHO standard for 50% VEs even in the Delta dominated periods, despite the VEs waning over time as the Delta variant dominated. Our results on real-world VE were largely agreeable to those of the published studies via clinical trials and retrospective studies with smaller sample size and higher costs. As demonstrated in the scenario analysis in Section 7, the proposal estimation approach can be used to simulate outcomes under various vaccination strategies, for instance doubling the vaccination rates of the first dose for a more intensive version of the first-dose-priority, in an effort to find better strategies than the one having been carried out by the countries. Our finding of higher effectiveness of the full vaccination would support efforts for the boost vaccine uptake in the population in the Omicron era.

Funding. The research was supported by NSFC Grants 12071013 and 92046021.

SUPPLEMENTARY MATERIAL

Supplementary Material to "Estimating COVID-19 Vaccine Efficacy via Dynamic Epidemiological Models–A Study of Ten Countries"
The supplementary material provides the additional details, tables and figures.

REFERENCES

ANDERSON, R. and MAY, R. (1982). Population dynamics of human helminth infections: Control by chemotherapy. *Nature* **297** 557-63. https://doi.org/10.1038/297557a0

AURANEN, K., ARJAS, E., LEINO, T. et al. (2000). Transmission of pneumococcal carriage in families: a latent Markov process model for binary longitudinal data. *Journal of the American Statistical Association* **95** 1044–1053.

BAAKE, E., BAAKE, M., BOCK, H. G. et al. (1992). Fitting ordinary differential equations to chaotic data. *Physical Review A* **45** 5524–5529. https://doi.org/10.1103/PhysRevA.45.5524

BECKER, N. G. (1997). Uses of the EM algorithm in the analysis of data on HIV/AIDS and other infectious diseases. *Statistical Methods in Medical Research* **6** 24–37.

BERNAL, J. L., ANDREWS, N., GOWER, C. et al. (2021). Effectiveness of Covid-19 Vaccines against the B.1.617.2 (Delta) Variant. *New England Journal of Medicine* **385** 585-594. https://doi.org/10.1056/NEJMoa2108891

BUITRAGO-GARCIA, D., EGLI-GANY, D., COUNOTTE, M. et al. (2020). Occurrence and transmission potential of asymptomatic and presymptomatic SARS-CoV-2 infections: A living systematic review and meta-analysis. *PLoS medicine* **17** e1003346. https://doi.org/10.1371/journal.pmed.1003346

CAI, C., LIU, Y., ZENG, S. et al. (2021a). The efficacy of COVID-19 vaccines against the B.1.617.2 (delta) variant. *Molecular Therapy* **29** 2890–2892. https://doi.org/10.1016/j.ymthe.2021.09.024

CAI, C., PENG, Y., SHEN, E. et al. (2021b). A comprehensive analysis of the efficacy and safety of COVID-19 vaccines. *Molecular Therapy* **29** 2794–2805. https://doi.org/10.1016/j.ymthe.2021.08.001

DASHTBALI, M. and MIRZAIE, M. (2021). A compartmental model that predicts the effect of social distancing and vaccination on controlling COVID-19. *Scientific Reports* **11** 1–11.

DORIA-ROSE, N., SUTHAR, M. S., MAKOWSKI, M. et al. (2021). Antibody Persistence through 6 Months after the Second Dose of mRNA-1273 Vaccine for Covid-19. *New England Journal of Medicine* **384** 2259-2261. https://doi.org/10.1056/NEJMc2103916

DUKIC, V., LOPES, H. F. and POLSON, N. G. (2012). Tracking Epidemics With Google Flu Trends Data and a State-Space SEIR Model. *Journal of the American Statistical Association* **107** 1410–1426.

GIORDANO, G., COLANERI, M., DI FILIPPO, A. et al. (2021). Modeling vaccination rollouts, SARS-CoV-2 variants and the requirement for non-pharmaceutical interventions in Italy. *Nature Medicine* **27** 993–998.

GU, J., YAN, H., HUANG, Y. et al. (2020). Comparing containment measures among nations by epidemiological effects of COVID-19. *National Science Review* **7** 1847-1851. https://doi.org/10.1093/nsr/nwaa243

GUAN, W., NI, Z., HU, Y. et al. (2020). Clinical Characteristics of Coronavirus Disease 2019 in China. *New England Journal of Medicine* **382** 1708-1720. https://doi.org/10.1056/NEJMoa2002032

HAO, X., CHENG, S., WU, D. et al. (2020). Reconstruction of the full transmission dynamics of COVID-19 in Wuhan. *Nature* **584** 420–424.

HICKS, G. and RAY, W. (1971). Approximation methods for optimal control synthesis. *The Canadian Journal of Chemical Engineering* **49** 522–528.

HOLLAND, J. H. (1992). Genetic algorithms. *Scientific American* **267** 66–73.

JOHNSON & JOHNSON (2021). Positive New Data for Johnson & Johnson Single-Shot COVID-19 Vaccine on Activity Against Delta Variant and Long-lasting Durability of Response. https://www.jnj.com/positive-new-data-for-johnson-johnson-single-shot-covid-19-vaccine-on-activity-against-delta-variant-and-long-lasting-durability-of-response.

KERMACK, W. O. and MCKENDRICK, A. G. (1927). A contribution to the mathematical theory of epidemics. *Proceedings of the Royal Society of London. Series A, Containing papers of a mathematical and physical character* **115** 700–721. https://doi.org/10.1098/rspa.1927.0118

LI, X., HUANG, Y., WANG, W. et al. (2021). Effectiveness of inactivated SARS-CoV-2 vaccines against the Delta variant infection in Guangzhou: a test-negative case–control real-world study. *Emerging Microbes & Infections* **10** 1751-1759. https://doi.org/10.1080/22221751.2021.1969291

LIANG, H. and WU, H. (2008). Parameter Estimation for Differential Equation Models Using a Framework of Measurement Error in Regression Models. *Journal of the American Statistical Association* **103** 1570-1583. https://doi.org/10.1198/016214508000000797

LIU, C., GINN, H. M., DEJNIRATTISAI, W. et al. (2021). Reduced neutralization of SARS-CoV-2 B.1.617 by vaccine and convalescent serum. *Cell* **184** 4220–4236. https://doi.org/10.1016/j.cell.2021.06.020

PLANAS, D., VEYER, D., BAIDALIUK, A. et al. (2021). Reduced sensitivity of SARS-CoV-2 variant Delta to antibody neutralization. *Nature* **596** 276–280. https://doi.org/10.1038/s41586-021-03777-9

POLACK, F. P., THOMAS, S. J., KITCHIN, N. et al. (2020). Safety and Efficacy of the BNT162b2 mRNA Covid-19 Vaccine. *New England Journal of Medicine* **383** 2603-2615. https://doi.org/10.1056/NEJMoa2034577

QUICK, C., DEY, R. and LIN, X. (2021). Regression Models for Understanding COVID-19 Epidemic Dynamics With Incomplete Data. *Journal of the American Statistical Association* **116** 1561-1577. https://doi.org/10.1080/01621459.2021.2001339

RAMSAY, J., HOOKER, G., CAMPBELL, D. et al. (2007). Parameter Estimation for Differential Equations: A Generalized Smoothing Approach. *Journal of the Royal Statistical Society Series B* **69** 741–796. https://doi.org/10.1111/j.1467-9868.2007.00610.x

SHEIKH, A., MCMENAMIN, J., TAYLOR, B. et al. (2021). SARS-CoV-2 Delta VOC in Scotland: demographics, risk of hospital admission, and vaccine effectiveness. *The Lancet* **397** 2461–2462. https://doi.org/10.1016/S0140-6736(21)01358-1

TIAN, T., TAN, J., LUO, W. et al. (2021). The Effects of Stringent and Mild Interventions for Coronavirus Pandemic. *Journal of the American Statistical Association* **116** 481-491. https://doi.org/10.1080/01621459.2021.1897015

VOYSEY, M., CLEMENS, S. A. C., MADHI, S. A. et al. (2021). Safety and efficacy of the ChAdOx1 nCoV-19 vaccine (AZD1222) against SARS-CoV-2: an interim analysis of four randomised controlled trials in Brazil, South Africa, and the UK. *The Lancet* **397** 99–111. https://doi.org/10.1016/S0140-6736(20)32661-1

WHO (2021). What is COVID-19 vaccine efficacy. https://www.afro.who.int/news/what-covid-19-vaccine-efficacy.

YAN, H., ZHU, Y., GU, J. et al. (2021). Better strategies for containing COVID-19 pandemic: a study of 25 countries via a vSIADR model. *Proceedings of the Royal Society A* **477** 20200440. https://doi.org/10.1098/rspa.2020.0440